Towards Robust Parameterizations in Ecosystem-level Photosynthesis Models

Shanning Bao[1,1,1], Lazaro Alonso[2,2,2], Siyuan Wang[3,3,3], Johannes Gensheimer[2,2,2], Ranit De[2,2,2], and Nuno Carvalhais[3,3,3]

[1]National Space Science Center Chinese Academy of Sciences
[2]Max-Planck Institute for Biogeochemistry
[3]Max-Planck-Institute for Bio-geochemistry

August 11, 2023

Abstract

In a model simulating dynamics of a system, parameters can represent system sensitivities and unresolved processes, therefore affecting model accuracy and uncertainty. Taking a light use efficiency (LUE) model as an example, which is a typical approach to estimate gross primary productivity (GPP), we propose a Simultaneous Parameter Inversion and Extrapolation approach (SPIE) to overcome issues stemming from plant-functional-type(PFT)-dependent parameterizations. SPIE refers to predicting model parameters using an artificial neural network based on collected variables, including PFT, climate types, bioclimatic variables, vegetation features, atmospheric nitrogen and phosphorus deposition and soil properties. The neural network was optimized to minimize GPP errors and constrain LUE model sensitivity functions. We compared SPIE with 11 typical parameter extrapolating methods, including PFT- and climate-specific parameterizations, global and PFT-based parameter optimization, site-similarity, and regression approaches. All methods were assessed using Nash-Sutcliffe model efficiency(NSE), determination coefficient and normalized root mean squared error, and contrasted with site-specific calibrations. Ten-fold cross-validated results showed that SPIE had the best performance across sites, various temporal scales and assessing metrics. None of the approaches performed similar to site-level calibrations(NSE=0.95), but SPIE was the only approach showing positive NSE(0.68). The Shapley value, layer-wise relevance and partial dependence showed that vegetation features, bioclimatic variables, soil properties and some PFTs are determining parameters. The proposed parameter extrapolation approach overcomes strong limitations observed in many standard parameterization methods. We argue that expanding SPIE to other models overcomes current limits and serves as an entry point to investigate the robustness and generalization of different models.

Hosted file

`essoar.10512186.3.docx` available at https://authorea.com/users/644037/articles/598288-towards-robust-parameterizations-in-ecosystem-level-photosynthesis-models

Towards Robust Parameterizations in Ecosystem-level Photosynthesis Models

Shanning Bao[1,2*], Lazaro Alonso[1], Siyuan Wang[1], Johannes Gensheimer[1], Ranit De[1], Nuno Carvalhais[1,3,4*]

[1]Department for Biogeochemical Integration, Max-Planck-Institute for Biogeochemistry, 07745, Jena, Germany.

[2]National Space Science Center, Chinese Academy of Sciences, 100190, Beijing, China.

[3]Departamento de Ciências e Engenharia do Ambiente, DCEA, Faculdade de Ciências e Tecnologia, FCT, Universidade Nova de Lisboa, 2829-516 Caparica, Portugal.

[4]ELLIS Unit Jena, 07745, Jena, Germany.

Corresponding authors: Shanning Bao (baoshanning@nssc.ac.cn) and Nuno Carvalhais (ncarvalhais@bgc-jena.mpg.de)

Key Points:

- We propose a machine-learning-based parameterization method to model gross primary productivity
- The method overcomes significant biases in predictions using assumptions of biome-dependent and globally fixed parameterizations
- Vegetation, climate and soil properties explain most variability in model parameters, challenging current prescriptions of their patterns.

Abstract

In a model simulating dynamics of a system, parameters can represent system sensitivities and unresolved processes, therefore affecting model accuracy and uncertainty. Taking a light use efficiency (LUE) model as an example, which is a typical approach to estimate gross primary productivity (GPP), we propose a Simultaneous Parameter Inversion and Extrapolation approach (SPIE) to overcome issues stemming from plant-functional-type(PFT)-dependent parameterizations. SPIE refers to predicting model parameters using an artificial neural network based on collected variables, including PFT, climate types, bioclimatic variables, vegetation features, atmospheric nitrogen and phosphorus deposition and soil properties. The neural network was optimized to minimize GPP errors and constrain LUE model sensitivity functions. We compared SPIE with 11 typical parameter extrapolating methods, including PFT- and climate-specific parameterizations, global and PFT-based parameter optimization, site-similarity, and regression approaches. All methods were assessed using Nash-Sutcliffe model efficiency(NSE), determination coefficient and normalized root mean squared error, and contrasted with site-specific calibrations. Ten-fold cross-validated results showed that SPIE had the best performance across sites, various temporal scales and assessing metrics. None of the approaches performed similar to site-level calibrations(NSE=0.95), but SPIE was the only approach showing positive NSE(0.68). The Shapley value, layer-wise relevance and partial dependence showed that vegetation features, bioclimatic variables, soil properties and some PFTs are determining parameters. The proposed parameter extrapolation approach overcomes strong limitations observed in many standard parameterization methods. We argue that expanding SPIE to other models overcomes current limits and serves as an entry point to investigate the robustness and generalization of different models.

Plain Language Summary

Parameters can represent ecosystem properties and sensitivities of ecosystem processes to environment changes, affecting model accuracy and outputs uncertainties. Therefore determining parameters is of great importance for applying models. Current ecosystem-level models mostly determine parameters according to biomes. For example, light use efficiency (LUE) models, a typical tool to estimate gross primary productivity (GPP), use plant-functional-type(PFT)-specific parameters. However, PFT-specific parameters cannot represent the spatial variance of GPP sensitivities to environmental conditions within PFT and introduce significant estimation errors. To overcome these issues, we propose a Simultaneous Parameter Inversion and Extrapolation method (SPIE). Taking an LUE model as an example, we estimated model parameters using SPIE based on the input features representing vegetation, climate and soil properties at 196 observational sites. We compared SPIE with 11 other parameter extrapolating methods and all these methods with site-specific calibrations based on full-time-series observed GPP. The results were validated and showed that SPIE was the best method to extrapolate parameters across various temporal and spatial scales. According to the importance of input features, vegetation, bioclimatic, soil properties and some PFTs are dominating spatial changes of parameters. Overall, SPIE is a robust method which overcomes strong limitations in many standard parameter extrapolating methods.

1 Introduction

Increasing studies based on model ensembles reveal that large uncertainties remain in modeling the global carbon cycle and ecosystem responses to environmental changes (Baldocchi,

Ryu, & Keenan, 2016; Bloom, Exbrayat, Van Der Velde, Feng, & Williams, 2016; Piao et al., 2020). The uncertainties are mainly due to various limitations in model structures, driver data and parameters (Huntzinger et al., 2017; Medlyn, Robinson, Clement, & McMurtrie, 2005; Zheng et al., 2018). Although model parameters contribute to considerable uncertainties, most global vegetation models are parameterized using fixed, biome- or plant functional type (PFT)-based values, which cannot capture the spatial variability of carbon assimilation processes (Bloom et al., 2016). The fixed and PFT-based parameterization are also widely used and introduced uncertainties in gross primary productivity (GPP) models (Groenendijk et al., 2011; Ryu, Berry, & Baldocchi, 2019), including light use efficiency (LUE) models, leaf-scale-process-based models, machine-learning and sun-induced fluorescence models (Frankenberg et al., 2011; Jung et al., 2011; Running et al., 2004; Tian et al., 2020; Zhang et al., 2012). A more robust and physically intuitive parameterization method is desired for constraining the global GPP estimation.

LUE models are typical approaches for the estimation of GPP at large global scales (Mahadevan et al., 2008; Potter et al., 1993; Running et al., 2004; Tian et al., 2020; Yuan et al., 2007). These kinds of models incorporate the knowledge of environmental constraints to the originally proposed empirical LUE model, Monteith et al.(1972)'s model, having advantages of high efficiency and algorithmic transparency compared to leaf-scale-process-based models and machine-learning-based models, respectively.

The first global GPP product based on MODIS LUE algorithm (Running et al., 2004) proposed a set of PFT-dependent parameters. Later, other published global LUE models inherit the PFT-based parameterization method or incorporate parameters directly extracted from literature (He et al., 2013; Mahadevan et al., 2008; Xiao et al., 2004; Xie & Li, 2020). The PFT-based approach is not exclusive to LUE models, but also commonly used in dynamic global vegetation models and the land surface schemes of global Earth system models supporting IPCC reports (Ciais et al., 2019; Masson-Delmotte et al., 2021; T. Stocker, 2014; Wenzel, Cox, Eyring, & Friedlingstein, 2014). However, applying parameterizations in locations or regions, which have not previously used for or evaluated against might easily lead to naïve conclusions about model structure robustness and/or parameter generalization. To overcome this limitation, LUE models usually calibrate parameters within their physical ranges to minimize the mismatch between the modeled and the observational GPP (Carvalhais et al., 2008; Horn & Schulz, 2011a; Mäkelä et al., 2008; Yan et al., 2017; Zhou et al., 2016), i.e., the GPP estimated from eddy covariance (EC) carbon flux. This method is supported by the availability of EC flux towers, but given the need for parameter generalization limited for the global domain. To parameterize the Carnegie-Ames-Stanford approach (CASA) model in locations without EC observations, Carvalhais et al (2010) considered *in situ* parameterizations from EC sites with the same PFT and similar climate and vegetation features. Other studies use the average site-level optimized parameters per PFT (Guan, Chen, Shen, Xie, & Tan, 2022; Yuan, Cai, Xia, et al., 2014; Zhou et al., 2016), PFT-specific optimized parameters (Tian et al., 2020; Zheng et al., 2020), globally optimized parameters (B. D. Stocker et al., 2020; Yuan et al., 2019) or globally fixed parameters (Mengoli et al., 2022; H. Wang et al., 2017). Yuan et al (2014) showed using six different LUE models that the modeled GPP using globally optimized parameters was not significantly different from that using PFT-specific optimized parameters. However, it has been illustrated that at least parameter variations between PFTs need to be considered to reach confident model performances (Tian et al., 2020). In general, most studies did not account for parameter variances within PFT,

despite assuming that LUE model parameters are related to characteristics of the vegetation and the environment.

In some studies, the drivers for spatial changes of model parameters were analyzed based on site-level calibrated parameters. For example, Horn et al (2011b) found that their LUE model parameters, which represent the maximum light use efficiency and the sensitivity of GPP to temperature and soil moisture, varied across climate zones and biomes and can be predicted using vegetation and environmental properties. The relationship between parameters and plant traits also existed in process-based GPP models (Peaucelle et al., 2019). Moreover, Luo et al (2020) claimed that model parameters, which can represent both the evolving ecosystem properties and the unresolved ecosystem processes, should be determined according to our knowledge about the changing ecosystem properties. All these studies confirmed the control of vegetation attributes and environmental features on model parameters, which represents GPP sensitivities. These findings inspire the possible next generation of parameterization methods based on the physical connection between model parameters and ecosystem properties.

In this study, we aim to propose a new model parameterization method (or parameter extrapolation method) that explicitly accommodates the contribution of PFT as well as other vegetation features and environmental conditions to parameter spatial variability. We allow the spatial variation of parameters, indicating GPP sensitivities to environmental forcings, to be learned from a set of ecosystem properties. To test the approach, we compared 12 different parameterization methods (see details in section 2.2) based on an exemplified LUE model with appropriate environmental drivers and sensitivity functional forms selected from an ensemble of 5600 LUE models (Bao et al., 2022). These parameterization methods were assessed according to the accuracy of the simulated GPP (GPP_{sim}) across different time scales at the site level, per PFT, per climate type and globally (see section 2.3). The importance of drivers for model parameters was evaluated using three different methods (see section 2.4).

2 Materials and Methods

2.1 Light use efficiency model

LUE models define GPP as a product of the photosynthetically active radiation (PAR), the fraction of photosynthetically active radiation (FAPAR) and the maximum light use efficiency ($\boldsymbol{\varepsilon_{max}}$), regulated by environmental sensitivity functions. The environmental drivers and sensitivity functional forms differ across LUE models. To minimize the selection effect of environmental drivers and sensitivity functions, we select an LUE model based on Bao et al. (2022) which considers the impacts of temperature (T), vapor pressure deficit (VPD), atmospheric CO_2 concentration (c_a), soil moisture (W), light intensity (L) and the cloudiness index (CI) on GPP dynamics (see equations 1-8).

$$\mathrm{GPP}=\mathrm{PAR}\cdot\mathrm{FAPAR}\cdot\boldsymbol{\varepsilon_{max}}\cdot f\mathrm{T}\cdot f\mathrm{VPD}\cdot f\mathrm{W}\cdot f\mathrm{L}\cdot f\mathrm{CI} \tag{1}$$

$$f\mathrm{T}=\frac{2e^{-\left(\mathrm{T_f}-\mathbf{T_{opt}}\right)/\mathbf{k_T}}}{1+e^{\left(-\left(\mathrm{T_f}-\mathbf{T_{opt}}\right)/\mathbf{k_T}\right)^2}} \tag{2}$$

$$f\mathrm{VPD}=e^{\boldsymbol{\kappa}\left(\frac{\mathbf{C_{a0}}}{c_a}\right)^{\mathbf{C}_{\boldsymbol{\kappa}}}\mathrm{VPD}}\left(1+\frac{c_a-\mathbf{C_{a0}}}{c_a-\mathbf{C_{a0}}+\mathbf{C_m}}\right) \tag{3}$$

$$fW=\frac{1}{1+e^{\mathbf{k_W}(\mathbf{k_W}-\mathbf{W_I})}} \quad (4)$$

$$fL=\frac{1}{1+\gamma\cdot APAR} \quad (5)$$

$$fCI=CI^{\boldsymbol{\mu}} \quad (6)$$

$$T_f(t)=(1-\boldsymbol{\alpha_T})\cdot T(t)+\boldsymbol{\alpha_T}\cdot T_f(t-1) \quad (7)$$

$$T_f(t)=(1-\boldsymbol{\alpha_W})\cdot W(t)+\boldsymbol{\alpha_W}\cdot W_f(t-1) \quad (8)$$

The LUE model includes 13 parameters in total (in **bold**). All sensitivity functions (*f*T, *f*VPD, *f*W, *f*L and *f*CI) are scaled from zero to one, representing from strong to no constraints. The physical meanings and units of the parameters and references of these sensitivity functions are summarized in Table 1.

Table 1. List of LUE model parameters

Parameters	Meanings	Range	Units	References
$\boldsymbol{\varepsilon_{max}}$	Maximum light use efficiency	0 – 10	$gC\cdot MJ^{-1}$	(Running et al., 2004)
$\mathbf{T_{opt}}$	Optimal temperature	5 – 35	°C	(Horn & Schulz, 2011a)
$\mathbf{k_T}$	Sensitivity to temperature changes	1 – 20	-	
$\boldsymbol{\kappa}$	Sensitivity to vapor pressure deficit changes	-10^{-1} – -10^{-4}	kPa^{-1}	(Mäkelä et al., 2008)
$\mathbf{C_{a0}}$	Minimum optimal atmospheric CO_2 concentration	340 – 390	ppm	(Kalliokoski, Makela, Fronzek, Minunno, & Peltoniemi, 2018)
$\mathbf{C_\kappa}$	Sensitivity to atmospheric CO_2 concentration changes	0 – 10	-	
$\mathbf{C_m}$	CO_2 fertilization intensity indicator	100 – 4000	ppm	
$\mathbf{k_W}$	Sensitivity to soil moisture changes	-30 – -5	-	(Horn & Schulz, 2011a)
$\mathbf{W_I}$	Optimal soil moisture	0.01 – 0.99	$cm\cdot cm^{-1}$	
$\boldsymbol{\gamma}$	Light saturation curvature indicator	0 – 1	$MJ^{-1}\cdot m^2\cdot d$	(Mäkelä et al., 2008)
$\boldsymbol{\mu}$	Sensitivity to cloudiness index changes	10^{-3} – 1	-	(Bao et al., 2022)
$\boldsymbol{\alpha_T}$	Lag parameter for temperature effect	0.0 – 0.9	-	(Horn & Schulz, 2011a)
$\boldsymbol{\alpha_W}$	Lag parameter for soil moisture effect	0.0 – 0.9	-	

The sensitivity function of VPD, *f*VPD, includes the effect of both VPD and c_a, which jointly control the leaf internal CO_2 concentration. The pure CO_2 fertilization effect is described only by the right part of *f*VPD (i.e., the sum of one and c_a function). The product of PAR and FAPAR, i.e., the absorbed photosynthetically active radiation (APAR), is the estimate of the light energy intercepted by the vegetation canopy, and thus was used as the light intensity input

of the sensitivity function of L (fL). The T and W were temporally filtered using lag parameters, $\boldsymbol{\alpha}_{\mathbf{T}}$ and $\boldsymbol{\alpha}_{\mathbf{W}}$, at boreal and arid regions, respectively, according to Horn et al (2011a).

2.1.1 Forcing data and parameter calibration

The forcing data for the LUE model was collected at 196 EC sites (listed in Table S1) from FLUXNET (www.fluxnet.org). The detailed sources and algorithms of the forcing data are summarized in Table S2. The GPP estimated from the observed net ecosystem exchange (NEE) at EC sites (GPP_{obs}) were also collected to calibrate parameters and evaluate parameterization methods.

In the parameter calibration process, we added constraints on GPP simulation errors and sensitivity functions (e.g., fT) following the concept of ecological and dynamic constraints (see details in section S1). As a derivative-free global searching algorithm, CMAES (Hansen & Kern, 2004), was used to search the optimal parameters in its physical range according to the full time series of GPP_{obs}. We assumed that the simulated GPP using the optimized parameters (GPP_{calib}) can reach the model potential (i.e., the highest model performance) with GPP_{calib} considered as a reference for its good fitness to GPP_{obs}.

2.1.2 Input features for predicting parameters

To extrapolate the parameters across various sites and in the future to the global scale, we collect mainly the variables that can represent the ecosystem properties available at both local (i.e., site-level) and global scales. These variables include the PFT, climate classification types (Clim; Rubel, Brugger, Haslinger, & Auer, 2017), 19 bioclimatic variables (BIO1-19, classified as 'BioClim'; Xu & Hutchinson, 2011), two aridity features (AI1-2, classified as ‘BioClim’), 11 vegetation index features (VIF1-11, represented by ‘VIF’), atmospheric Nitrogen and Phosphorus deposition (NdepNHX, NdepNOY and Pdep, summarized as 'NPdep'; R. Wang et al., 2017) and 17 soil properties (classified as 'Soil'; Poggio et al., 2021). In other words, we totally used six classes of input features which are shorted to BioClim, Clim, NPdep, PFT, Soil and VIF. The details of the input features are summarized in Table S3.

The categorical variables (PFT and climate types) were converted to one or zero to indicate whether the target location belongs to a specific type or not. All non-categorical variables were normalized by subtracting the mean of each feature and dividing by the standard deviation (equation 9). The original and normalized features are represented by *var* and var_{nor}. The mean and standard deviation per feature are represented by *mean* and *std*, respectively.

$$var_{\mathrm{nor}}=\frac{var\text{-}mean}{std} \tag{9}$$

2.2 Parameterization methods

We extrapolate the parameters based on a ten-fold cross-validation strategy using the collected input features. Namely, the samples, here refers to the EC sites, were divided into 10 groups randomly (see the group number of each site in Table S1). We trained the parameterization models using nine of 10 groups and validate the result using the one left, and repeated 10 times until getting validated results from all sites. All PFT and climate classification types (11 PFT and 14 climate classification types in total, see Table S1) were included in each training dataset.

The 12 parameterization methods can be divided into six groups, i.e., univariate clustering, similarity-based, optimization-based, regression-based, our hybrid approach based on a neural network and globally-fixed methods (see details in sections 2.2.1-2.2.6).

2.2.1 Univariate clustering methods (‘PFTmean’, ‘Climmean’, ‘PFTmed’, and ‘Climmed’)

In regions without observational data, the parameters were determined by the arithmetic mean from the calibrated parameters at the sites with the same PFT (Guan et al., 2022; Yuan, Cai, Xia, et al., 2014; Zhou et al., 2016). Here we tested the methods using the mean and median parameters per PFT and climate type.

‘PFT_{mean}’: means for calibrated parameter vectors per PFT;

‘$Clim_{mean}$’: means for calibrated parameter vectors per main climate type;

‘PFT_{med}’: medians for calibrated parameter vectors per PFT;

‘$Clim_{med}$’: medians for calibrated parameter vectors per main climate type.

2.2.2 Similarity-based method (‘Sitesim’)

The site similarity is defined by Carvalhais et al. (2010) which measures the similarity (D) of the climate and vegetation features between site *i* and site *j* as in equation 10:

$$D_{i,j}=1-\frac{\sum_{n=1}^{N}\left(\boldsymbol{V}_{i,n}-\boldsymbol{V}_{j,n}\right)^2}{\sum_{n=1}^{N}\left(\boldsymbol{V}_{i,n}-\bar{\boldsymbol{V}}_i\right)^2} \quad 10$$

Here, $\boldsymbol{V}$ is a vector including the normalized daily mean of the air temperature, precipitation (in logarithm), global radiation and LANDSAT-based normalized difference vegetation index (NDVI, see data source and processing method in Table S2) between 1986 and 2015.

To determine the parameters of a target location, we calculated D for each training site within the same PFT as the target location. The parameter vector at the site with the maximum D was used.

‘$Site_{sim}$’: parameter vectors for each site from the most similar site.

2.2.3 Optimization-based methods (‘OPT-All’ and ‘OPT-PFT’)

The parameters can be optimized across all sites or at sites per PFT (Yuan, Cai, Liu, et al., 2014). Here we adopted the same algorithm, CMAES, and the same cost functions as the site-specific calibration method (see section S1).

‘OPT-All’: a parameter vector optimized using all sites in the training dataset. (Yuan, Cai, Liu, et al., 2014)

‘OPT-PFT’: parameter vectors per PFT optimized using the sites within the same PFT in the training dataset (Kuppel et al., 2012; Tian et al., 2020).

2.2.4 Regression-based methods (‘sRF’, ‘mRF’, ‘mNN’)

To test the assumption that calibrated parameters are determined by ecosystem properties, here we predict the calibrated parameters using the normalized features based on different regression methods.

‘sRF’: parameter vectors per site of which each parameter was predicted independently based on the single-output random forest (trees number=100; Breiman, 2001).

‘mRF’: parameter vectors per site predicted simultaneously based on the multi-output random forest (trees number=100; Pedregosa et al., 2011).

‘mNN’: parameter vectors per site predicted simultaneously based on the multi-layer perceptron neural network (hidden layers number=2, neurons number=16; Gardner & Dorling, 1998; McCulloch & Pitts, 1943).

2.2.5 Simultaneous parameter inversion and extrapolation based on ecosystem properties (‘SPIE’)

Models can suffer from equifinality problems, namely different parameter vectors can generate similar model performance. Consequently, the calibrated parameters may not represent the true parameters to simulate GPP, which reflect the GPP sensitivities controlled by the environmental properties. Here we additionally test the assumption that the predicted parameter vector based on ecosystem properties, which might differ from the calibrated parameter vector, can simulate GPP with good accuracy. Instead of directly predicting parameters, we applied the neural network to predict GPP based on the LUE model using parameters predicted by the input features. The flowchart for this method is shown in Figure 1.

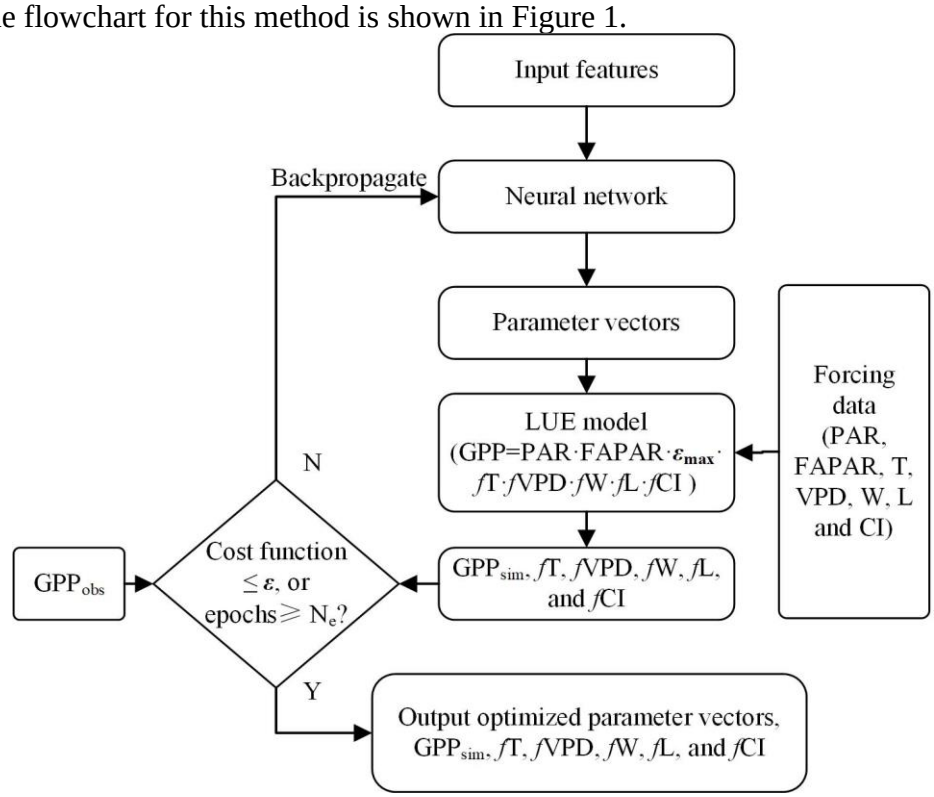

Figure 1. Flowchart of the GPP-targeting method. The parameter vectors per site are optimized until the cost function (see the definition in section S2) value is lower than the threshold ($\varepsilon=10^{-2}$) or epochs are more than the maximum epochs ($N_e=2\times10^3$).

First, the neural network predicts the parameter vectors based on the normalized features. The GPP_{sim} is then simulated using the predicted parameter vectors and compared with GPP_{obs} to measure the model error (see the definition in section S2). The neural network backpropagates the error to each hidden layer and optimizes the weight and bias of each neuron using ADAM algorithm (Kingma & Ba, 2014). We repeated the optimization process until the epochs reach 2×10^3. We set the learning rate ($=10^{-3}$), L_2 regularization coefficient ($=10^{-4}$), mini-batch size (=32), neurons per layer (=16) and hidden layers (=2) according to a grid-searching experiment (not shown here). We further applied a drop-out strategy (Srivastava, Hinton, Krizhevsky, Sutskever, & Salakhutdinov, 2014) to the input and hidden layers to reduce overfitting problems. The outputs from the network include the simulated GPP, sensitivity functions and predicted parameter vectors per site.

'SPIE': parameter vectors per site predicted based on ecosystem properties by minimizing GPP errors and constraining sensitivity functions of the LUE model.

2.2.6 Globally-fixed method ('P-model')

The derived P-model (B. D. Stocker et al., 2020; H. Wang et al., 2017) based on Farquhar et al (1980) and Fick's law together with an optimality theory (Prentice, Dong, Gleason, Maire, & Wright, 2014) adopts a globally-fixed parameter vector upscaled from leaf-scale processes. Mengoli et al (2022) improved the model by adding an acclimation process to the photosynthetic parameters. Here we ran the Mengoli model based on daily data, which is the same as the inputs for the selected LUE model (section 2.1.1), using the optimal parameters given in the paper (acclimation window size=15, running-mean approach based on daily data; Mengoli et al., 2022) and compared the model outputs, GPP, with other methods.

'P-model': a globally-fixed parameter vector from paper.

2.3 Statistical analysis for parameterized results

All the parameterization methods were assessed according to the GPP accuracy measured by Nash-Sutcliffe model efficiency (NSE, $(-\infty,1]$; NSE=1 indicates a perfect model), determination coefficient (R^2, [0,1]; R^2=1 indicates a perfect model) and normalized root mean squared error (NRMSE, $[0,\infty)$; NRMSE=0 indicates a perfect model) which is equal to the root mean squared error divided by the mean observational variable (e.g., GPP_{obs}). Only good-quality data were used to calculate NSE, R^2 and NRMSE. Here the good-quality data refers to the input vector of which the quality assessment flags (see 'QA' and 'QC' in Table S2) are all higher than 0.8, including quality assessment flags of all meteorological inputs, vegetation index and GPP_{obs}. When aggregated to longer time scales, the good quality data means the average quality flags are all higher than 0.7 at the weekly and monthly scales, and 0.5 at the yearly scale. Besides, predicted parameters were compared to calibrated parameters to test if the model equifinality problem exists.

2.3.1 Site-level temporal GPP assessment

We forced the LUE model at the daily scale and got the daily GPP_{sim} as a result. The weekly, monthly and yearly GPP_{sim} and GPP_{obs} were calculated based on the mean daily GPP_{sim} and GPP_{obs}, respectively. These time series of site-level GPP at different time scales were evaluated using NSE, R^2 and NRMSE. The vectors of NSE, R^2 and NRMSE were compared across all sites, per PFT and climate types.

2.3.2 Spatial variability of GPP assessment

The site-mean GPP_{obs} across sites represent the spatial variance of GPP. We used NSE, R^2 and NRMSE to measure the accuracy of the site-mean GPP_{sim} compared with GPP_{obs} to evaluate the ability of these parameterization methods to capture the spatial variability of GPP.

2.3.3 Comprehensive assessment across spatio-temporal scales based on model likelihood

The likelihood of each parameterization method, ***P***, was calculated according to Bao et al (2022). To avoid selecting a method falling shortly at locally describing ecosystem GPP, ***P*** represents an overall performance at 200 different site groups. In each group, 100 sites were selected randomly from all sites and two-years GPP were then randomly extracted from each of these 100 sites. The 200 site-years GPP_{sim} were compared to GPP_{obs} based on NSE, R^2 and NRMSE at each site-year independently. The differences between the daily, weekly, and monthly NSE, R^2 and NRMSE vectors and the yearly NRMSE vectors per parameterization method (each with 200 elements) were tested using Kolmogorov-Smirnov statistical test and t-test. The method with statistically higher NSE, R^2 or lower NRMSE than others was given with the largest score (=1, otherwise =0) at each site group. In case that two or more methods were statistically equal and better than others, NSE, R^2 or NRMSE across all site-years was additionally computed to sort these methods independently. ***P*** is equal to the average score across all site groups. The average ***P*** across different statistical metrics (NSE, R^2 and NRMSE) and time scales (daily, weekly, monthly and yearly) was used to detect the best parameterization method.

2.3.4 Comparison between predicted parameters and calibrated parameters

Since the 13 parameters have different meanings and ranges, they were compared independently. The similarity between the predicted parameters using methods introduced in section 2.2 and the calibrated parameters based on the observational data (see section S1) was assessed using NSE, R^2 and NRMSE.

2.4 Feature importance estimation

We evaluated the importance of input features using three methods and select the most important features based on the average normalized feature importance values.

2.4.1 Shapley-based feature importance (SHAP)

The Shapley value of a feature is calculated based on the deviation of the predicted parameter at a certain input from the average prediction (Lundberg & Lee, 2017), which represents the contribution of a feature to the output. Here SHAP is equal to the average absolute Shapley value across all inputs. The average SHAP across all cross-validation groups (Friedman, 2001) was used to assess the contribution of features for each parameter and all parameters.

2.4.2 Layer-wise-relevance-propagation-based feature importance (LRP)

The layer-wise relevance propagation refers to a strategy that allows decomposing the prediction of neural network over an input feature (Montavon, Binder, Lapuschkin, Samek, & Müller, 2019). It is usually used in deep classification neural networks, here we applied LRP to assess a shallow regression neural network. We calculated the relevance vector according to Bach et al. (2015) and measured the feature importance according to the average relevance across different cross-validation groups.

2.4.3 Partial-dependence-based feature importance (PD)

We estimated the partial dependence of the prediction on each input feature based on Friedman's (2001) algorithm. The feature importance, PD, was measured according to the partial dependence, which is equal to the standard deviation of the partial dependence if the input feature is non-categorical variables, otherwise is equal to the one-fourth of the absolute partial dependence range (Greenwell, Boehmke, & McCarthy, 2018).

3 Results

3.1 Temporal and spatial assessment

The parameterization method based on neural network aiming at minimizing GPP errors and constraining sensitivity functions, SPIE, had the best performance compared with other typical parameterization methods. All the assessing metrics at daily, weekly, monthly and yearly scales, NSE (Figure 2), R^2 (Figure S1) and NRMSE (Figure S2), showed that SPIE was better at more sites (i.e., more bright color blocks in Figure 2). The spatial variability of GPP can be also better captured by SPIE, which had higher NSE, R^2 and lower NRMSE measured by site-mean GPP_{obs} and GPP_{sim} (Figure 3). The accuracy of time series and site-mean GPP_{sim} using other methods were all significantly worse than SPIE. Although SPIE cannot perform as well as the site-specific calibration, it is the best parameter extrapolation method globally.

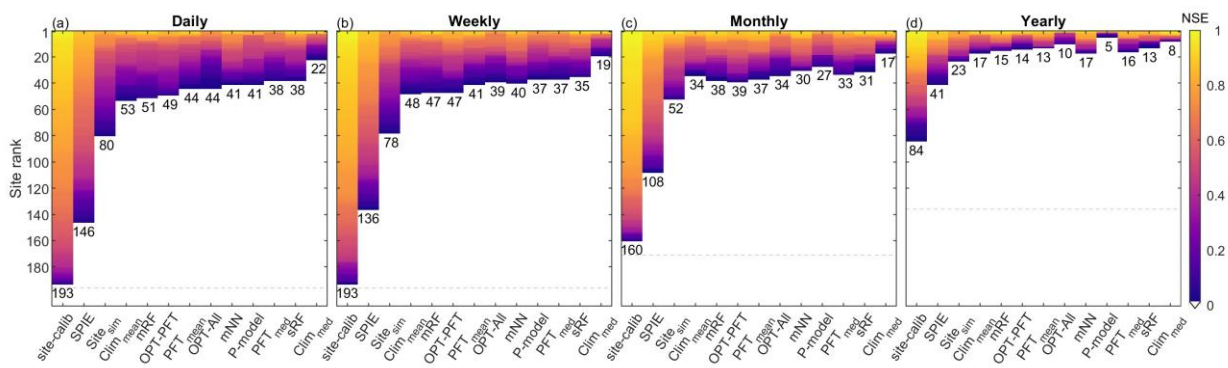

Figure 2. Comparison of NSE between GPP_{obs} and GPP_{sim} based on 12 different parameterization methods (see definitions of PFT_{mean}, $Clim_{mean}$, PFT_{med}, $Clim_{med}$, $Site_{sim}$, OPT-All, OPT-PFT, sRF, mRF, mNN, SPIE, and P-model in section 2.2), and between GPP_{obs} and GPP_{calib} (site-calib, see the calibration process in section S1) at daily (a), weekly (b), monthly (c) and yearly (d) scales. The methods are sorted according to the number of sites with positive NSE, which is displayed under each bar. The sites with negative NSE are in white color. The

area under the gray dashed line represents the sites excluded in the comparison due to less than four good-quality (see the definition of 'good-quality' data in section 2.3) data points.

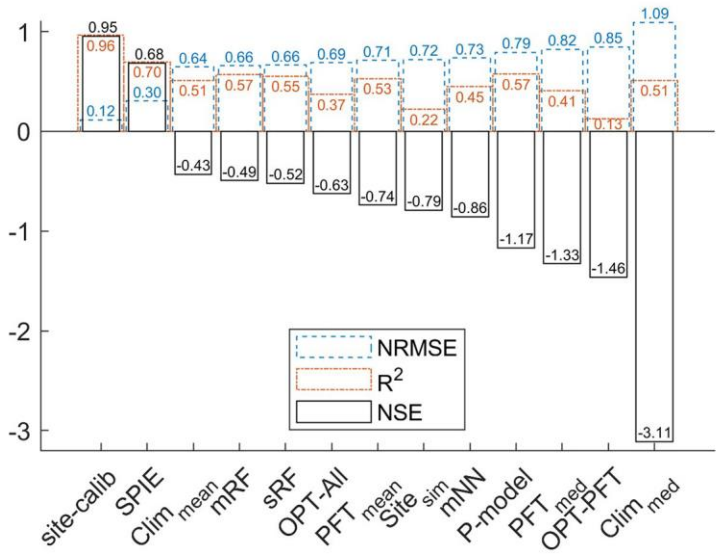

Figure 3. Comparison of NSE, R^2, and NRMSE between the site-mean GPP_{obs} and GPP_{sim}. The bars (i.e., parameterization methods) are sorted according to NSE.

The global best parameterization method, SPIE, outperformed across various PFTs and climate types. It had the highest daily NSE quantiles for each PFT and climate type considered in this study (Figure 4). While SPIE was relatively better than other methods, no extrapolated parameters can provide accurate GPP dynamics (NSE>0.4) at closed shrubland (Figure 4c), woody savanna (Figure 4l), tropical (Figure 4m) and polar (Figure 4q) climate types given that the model using calibrated parameters was good. It demonstrated that the variance of current extrapolated parameters was still insufficient and the parameters are possible to be overfitted in site calibrations. Using R^2 or NRMSE as the assessing metric (see details in Figure S3-4), the parameterization methods showed smaller but robust relative differences, i.e., the SPIE was still the best method. In general, while none of these parameter extrapolation methods can reach the highest model performance, SPIE was the best option for areas without observational data.

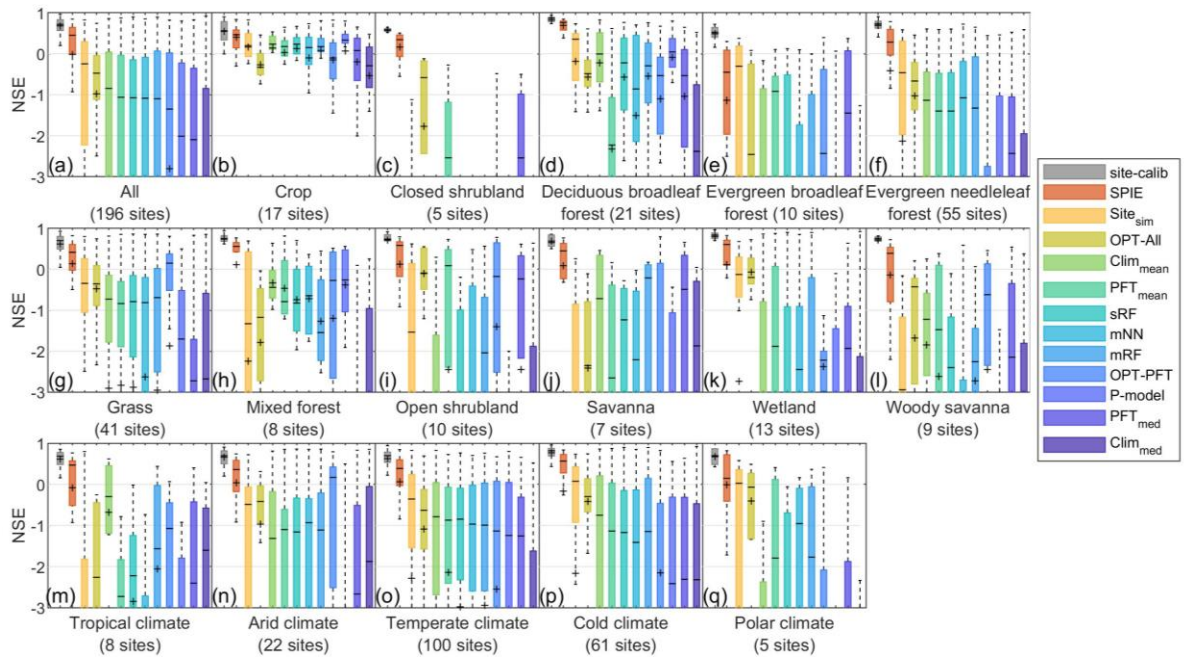

Figure 4. Site-level daily NSE comparison across all sites (a), per plant functional type (b-l) and climate type (m-q). The mean and median per type are represented by the black cross and the black line, respectively. The methods are sorted according to NSE medians across all sites. The area where NSE is lower than minus three is not displayed.

The model likelihood, ***P***, which represents the likelihood of a model statistically better than others across various site groups, illustrated that SPIE was the best method to extrapolate parameters, followed by OPT-All and $Clim_{med}$ with likelihoods lower than 0.06 (i.e., at less than 6% groups of sites the two methods can outperform). The average ***P*** of SPIE across daily, weekly, monthly, and yearly scales, and across various assessing metrics was also significantly higher than the other methods. It represented that the method is robust across various temporal and spatial scales.

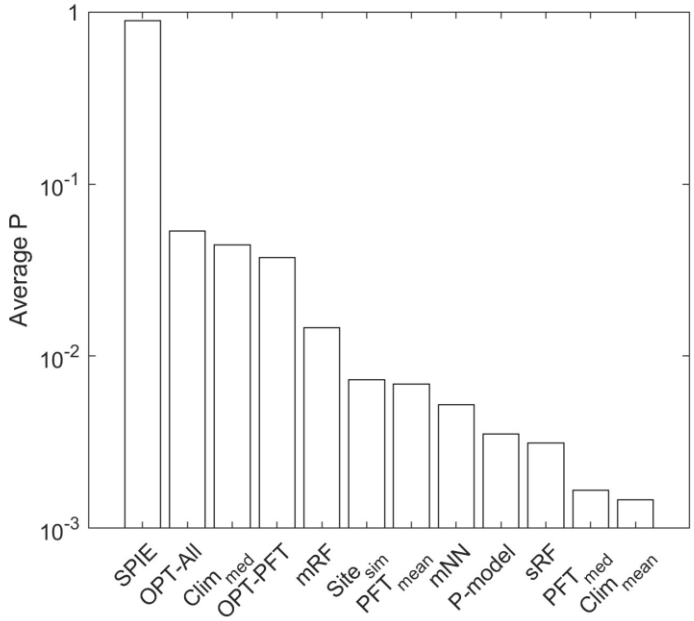

Figure 5. The average model likelihood (*P*) of parameterization methods

3.2 Differences between calibrated parameters and predicted parameters

The predicted parameters displayed different distribution patterns from the calibrated parameters. Taking the best method, SPIE, as an example (Figure 6), ranges of predicted parameters were narrower than calibrated parameters given the same predefined range. Further, SPIE predicted parameters had no 'edge-hitting' problem, which means that the parameter frequently reaches its maximum or minimum values, e.g., the calibrated parameters T_{opt}, k_T, C_κ, C_{a0}, C_m and k_W (Figure 6b-c, f-h, j). The other parameterization methods based on ecosystem properties (e.g., mRF, Figure S5) also showed narrower ranges. However, clustering and optimization-based methods had similar ranges to the site-calibrations and more edge-hitting instances than SPIE (see details in Figure S6-7).

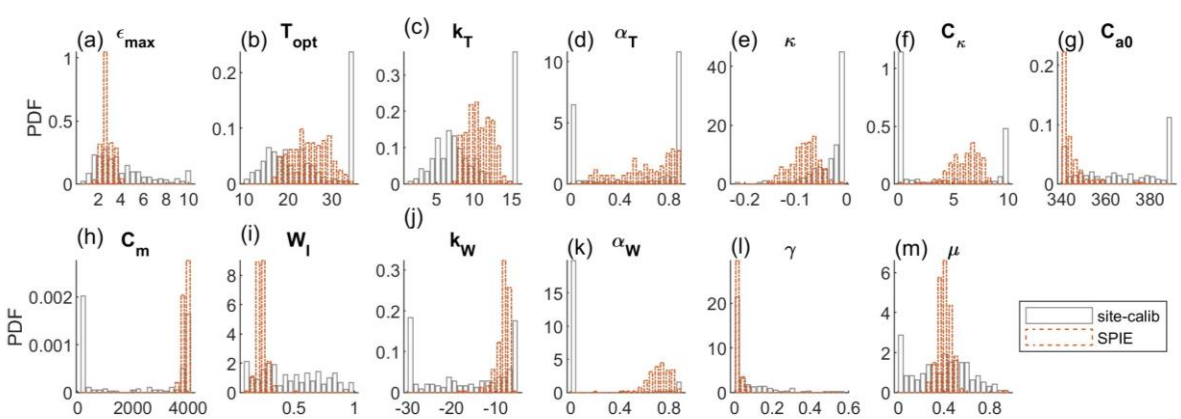

Figure 6. Probability density function (PDF) of the calibrated parameters (site-calib) and the predicted parameters by SPIE.

The LUE model performance was not determined by the parameter difference to site-specific calibrations. For example, NSE between the predicted parameters using SPIE and calibrated parameters across sites were all negative. The maximum R^2 was 0.08 and the lowest NRMSE was 0.08. Furthermore, the NSE difference between the calibration and SPIE was not correlated with the relative difference between calibrated and predicted parameters (Figure 7). Thus, the predicted parameters were not comparable to the calibrated parameters while they can produce similar GPP, suggesting the overfitting and parameter equifinality in the site-specific calibrations of LUE model.

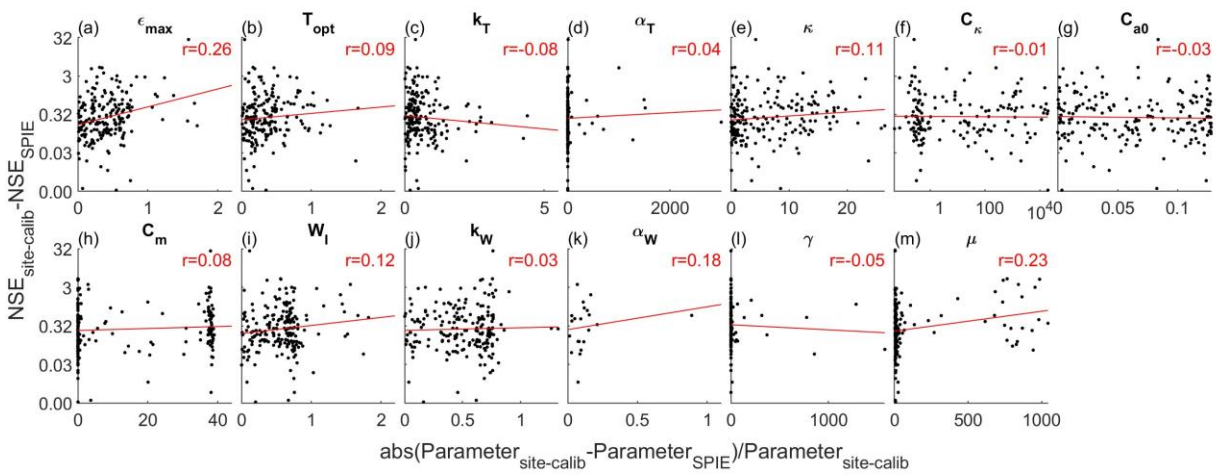

Figure 7. The distribution of site-level NSE differences between site-specific calibration ($NSE_{site\text{-}calib}$) and SPIE (NSE_{SPIE}) with the relative differences between calibrated parameters and predicted parameters. The red line is the least-squares fitting line of the scatters. The correlation coefficient (r) is displayed at the upper-right corner.

3.3 Important features for explaining model parameter variability

The average normalized values of SHAP, LRP and PD illustrated that vegetation index features, bioclimatic variables, soil properties and some PFTs were the most important variables explaining the spatial variability of model parameters (Figure 8). The importance values differed across three different methods, but all of them showed that most climate types were not important for determining model parameters (see details in Figure S8a-d). Some specific PFTs, e.g., DBF and MF, had the second and third highest importance values, indicating that their relative parameter vectors had different ranges compared to other PFTs. On average, the most important features were vegetation index features. Besides, most bioclimatic variables, soil properties and some specific PFTs were more important than other features.

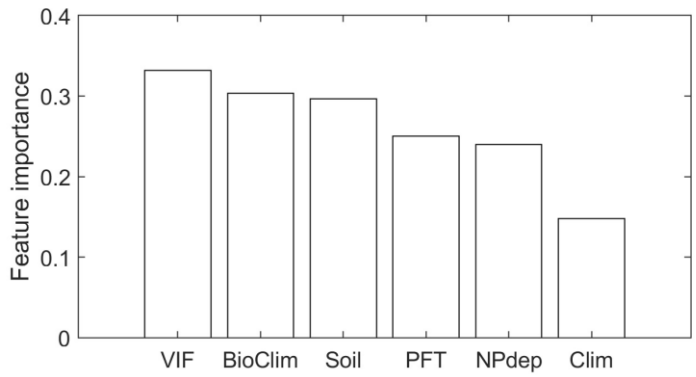

Figure 8. The input feature classes sorted by the average normalized SHAP, LRP and PD for all parameters. The detailed average SHAP, LRP and PD values for all parameters are displayed in Figure S8. The feature classes (see definitions in Table S3) refer to plant functional types (PFT), Koeppen-Geiger climate classification types (Clim), bioclimatic variables and aridity indexes (BioClim), vegetation index features (VIF), atmospheric nitrogen and phosphorus deposition (NPdep) and soil properties (Soil).

For a specific parameter, the most important feature was not the same as the one for all parameters. For example, $\boldsymbol{\varepsilon_{max}}$ was controlled mainly by AI1 (mean annual aridity index, see details in Figure S9), nonetheless W_I was controlled primarily by VIF7 (the range of mean annual EVI, see details in Figure S10). Although the ranks of input features were not clear across parameters and assessing methods, vegetation index features, bioclimatic variables, soil properties and some PFTs were shown to be determining the spatial variations of parameters that represent the GPP sensitivities to environment changes.

4 Discussion

4.1 Well-constrained site-specific parameterization is better than PFT-dependent parameterization

It has been shown that the long-used PFT-based parameterization cannot capture the variance in parameters within PFT (Bloom et al., 2016) and can be influenced by PFT misclassification errors. The method of directly using parameters from papers without local or global evaluation can be also risky. P-model which adopted the globally fixed parameters upscaled from the leaf scale might not include PFT errors (Mengoli et al., 2022; B. D. Stocker et al., 2020), but had limited accuracy across temporal (Figure 2) and spatial scales (Figure 3). Here, results showed that the globally fixed parameterization method (e.g., P-model) was worse than the PFT-based method (e.g., OPT-PFT, and PFT_{mean}). The global optimization method (e.g., OPT-All) had slightly better performance than PFT-based optimization at the global scale (Figure 5) due to a higher spatial generalizability (e.g., Figure 3), the same as Yuan et al (2014). However, OPT-All had accurate predictions at fewer sites (Figure 2). This agrees with a study using the PRELES model (Tian et al., 2020), which demonstrated that globally optimized parameters are not sufficient to reflect the variability of GPP sensitivities. Luo et al (2020) also confirmed that model parameters should vary with the spatial and temporal changes of ecosystem properties but not depend on PFTs. While the site-specific parameterizations ($Site_{sim}$, sRF, mRF, and mNN) have higher flexibility than clustering methods (PFT_{mean}, $Clim_{mean}$, PFT_{med}

and $Clim_{med}$), they did not show a robust advantage due to uncertainties remained in the calibrated parameters, which were used to constrain the predicted parameters in these methods. However, the site-specific parameterization constraining GPP prediction errors and sensitivity functions, SPIE, reaches the highest performance, highlighting that the well-constrained site-specific parameterization method can provide more reliable outputs than clustering and optimization methods. This is the opposite from the conclusion of Tian et al. (2020) who tested only the site-specific optimization method showing higher uncertainties than the PFT-based optimization method.

4.2 Reduced parameter variability by considering the relationship between parameters and ecosystem properties

Our results reveal the equifinality of model parameters, which consequently increases the model uncertainty. While no extrapolated parameter vectors outperformed calibrated ones, parameter ranges were better constrained in all methods based on ecosystem properties (e.g., sRF, mRF, mNN and SPIE) compared with site calibrations, clustering and optimization methods. The results of parameter distribution and GPP simulation performance demonstrate that considering physical links between GPP sensitivities and ecosystem properties can reduce the parameter equifinality and the overfitting in site-specific calibrations. This is also true in other LUE models (Horn & Schulz, 2011b). Furthermore, SPIE, considering only the GPP errors and constraints on sensitivity functions but not the distance to calibrated parameters, avoids inheriting uncertainties from model calibration. In general, the model parameterization relying on ecosystem properties can reduce the parameter uncertainty resulting from model equifinality.

4.3 Drivers of the spatial variability of GPP sensitivities

Overall, the information in vegetation features, bioclimatic variables, soil properties and some specific PFT (e.g., DBF and MF) explain most of the spatial variation in predicted parameters by SPIE. This general observation is similar to the results of other independent studies using a different LUE model (Horn & Schulz, 2011b) and terrestrial biosphere models (Peaucelle et al., 2019). Given our assumption that model parameters indicate GPP sensitivities, the results reflect the ecological understanding that vegetation features, bioclimatic conditions, soil properties along with plant forms impose instrumental controls on how ecosystems respond to environmental changes.

However, the current approach needs further development towards pinpointing key features controlling the spatial variability of parameters. On the one hand, strong covariation between input features (Figure S11) limits a confident variable attribution. While on the other hand, differences in variable importance between different methods (e.g., SHAP, LRP and PD) may result in different variable rankings (Figure S8). These may be associated to the covariation between features while also to the underlying assumptions per feature importance estimation method. However, given stationarity in the correlation structure between features, none of these aspects would limit a statistical extrapolation of parameter variability in space.

Differences in the model fitness between the site calibration and SPIE may reflect common overfitting issues in standard calibration exercises, challenging the generalization of a given GPP model and/or of features and architectures for the extrapolation approach. Exploring the contribution of additional variables may be a model-specific exercise, e.g., illumination

features, as in the model of Horn et al (2011b), that can contribute to the enhanced spatial variance in predicted parameters.

Given the background understanding that ecosystem properties, including vegetation features, climate regimes, soil characteristics and other environmental traits, influence response sensitivities of carbon assimilation fluxes to environmental conditions, our results suggest further expanding SPIE approach to other kinds of terrestrial ecosystem carbon cycle models (e.g., land surface models and dynamic global vegetation models). Yet, temporal changes in ecosystem properties can affect parameters (Luo & Schuur, 2020). Our results also suggest a cautionary remark on the temporal variation in parameters when extrapolating or applying parameters to long time scales (e.g., beyond decadal scales in prognostic simulations).

5 Conclusions

In this study, we developed a model parameterization approach based on the link between ecosystem sensitivities and properties constrained by GPP simulation errors and sensitivity functions. The method leverages on a neural network method to learn the parameterization of an LUE model. Moreover, the experimental design demonstrates that the method enables parameter extrapolation in regions without observational data with a significant and substantially higher accuracy than the widely-used PFT-based and globally fixed parameterization methods. Compared with a set of univariate clustering, similarity-, regression-based and fixed methods (NSE>0 at less than 41% of sites) considered in this study, our approach is unique in confidently predicting GPP fluxes in cross-validation (NSE>0 at 74% of sites). The resulting reduction in parameter variability by prediction via ecosystem properties suggests reductions in equifinality and overfitting commonly emerging from site-specific parameterizations. Vegetation features, bioclimatic variables, soil properties and some PFTs can explain the spatial variability of LUE model parameters. Overall, these are key features for diagnostic modeling exercises, although the temporal variation in the parameters and the relationship between them and ecosystem properties need to be further explored towards prognostic modeling. Given the general need for biological and ecological parameterizations in carbon and water terrestrial ecosystem models, our results propose statistical learning approaches for the parameterization of land surface schemes in Earth system models.

Acknowledgments

This work has received funding from the European Union's Horizon 2020 Research and Innovation Project DeepCube, under Grant Agreement Number 101004188, Youth Innovation Subject 2022 of National Space Science Center, Chinese Academy of Sciences, Sino-German (CSC-DAAD) Postdoc Scholarship Program and European Space Agency (ESA) via the Earth System Data Lab (ESDL) project. Lazaro Alonso and Johannes Gensheimer acknowledge the funding from European Research Council (ERC) Synergy Grant “Understanding and Modeling the Earth System with Machine Learning (USMILE)” (grant agreement No. 855187), and "Explainable AI pipelines for big Copernicus data" (grant agreement No. 101004188) under the Horizon 2020 research and innovation programme. This work used eddy covariance data acquired and shared by the FLUXNET community, including these networks: AmeriFlux, AfriFlux, AsiaFlux, CarboAfrica, CarboEuropeIP, CarboItaly, CarboMont, ChinaFlux, Fluxnet-Canada, GreenGrass, ICOS, KoFlux, LBA, NECC, OzFlux-TERN, TCOS-Siberia, and USCCC.

The FLUXNET eddy covariance data processing and harmonization was carried out by the ICOS Ecosystem Thematic Center, AmeriFlux Management Project and Fluxdata project of FLUXNET, with the support of CDIAC, and the OzFlux, ChinaFlux and AsiaFlux offices.

Data Availability Statement

Input data for light use efficiency model is available at the website of FLUXNET (https://fluxnet.org/). The FluxnetEO product is available from ICOS Carbon Portal https://doi.org/10.18160/0Z7J-J3TR (Walther et al., 2021a) for LANDSAT and https://doi.org/10.18160/XTV7-WXVZ (Walther et al., 2021b) for MODIS. CRUNCEP dataset for calculating bioclimatic variables is available at NCAR (https://rda.ucar.edu/datasets/ds314.3/#!description). Atmospheric nitrogen and phosphorus data is available at https://onlinelibrary.wiley.com/doi/abs/10.1111/gcb.13766. SoilGrids product is available at ftp://ftp.soilgrids.org/data/recent/. All data are also available by contacting the correspondence authors.

References

Bach, S., Binder, A., Montavon, G., Klauschen, F., Müller, K.-R., & Samek, W. (2015). On pixel-wise explanations for non-linear classifier decisions by layer-wise relevance propagation. *PLoS One*, *10*(7), e0130140.

Baldocchi, D., Ryu, Y., & Keenan, T. (2016). Terrestrial carbon cycle variability. *F1000Research*, *5*.

Bao, S., Wutzler, T., Koirala, S., Cuntz, M., Ibrom, A., Besnard, S., . . . Carvalhais, N. (2022). Environment-Sensitivity Functions for Gross Primary Productivity in Light Use Efficiency Models. *Agricultural and Forest Meteorology*, *312*, 108708. Retrieved from https://www.sciencedirect.com/science/article/pii/S0168192321003944. doi:https://doi.org/10.1016/j.agrformet.2021.108708

Bloom, A. A., Exbrayat, J.-F., Van Der Velde, I. R., Feng, L., & Williams, M. (2016). The decadal state of the terrestrial carbon cycle: Global retrievals of terrestrial carbon allocation, pools, and residence times. *Proceedings of the National Academy of Sciences*, *113*(5), 1285-1290.

Breiman, L. (2001). Random forests. *Machine learning*, *45*(1), 5-32.

Carvalhais, N., Reichstein, M., Collatz, G., Mahecha, M., Migliavacca, M., Neigh, C., . . . Seixas, J. (2010). Deciphering the components of regional net ecosystem fluxes following a bottom-up approach for the Iberian Peninsula. *Biogeosciences*, *7*(11), 3707-3729.

Carvalhais, N., Reichstein, M., Seixas, J., Collatz, G. J., Pereira, J. S., Berbigier, P., . . . Papale, D. (2008). Implications of the carbon cycle steady state assumption for biogeochemical modeling performance and inverse parameter retrieval. *Global Biogeochemical Cycles*, *22*(2).

Ciais, P., Tan, J., Wang, X., Roedenbeck, C., Chevallier, F., Piao, S.-L., . . . Canadell, J. (2019). Five decades of northern land carbon uptake revealed by the interhemispheric CO2 gradient. *Nature*, *568*(7751), 221-225.

Farquhar, G. D., von Caemmerer, S. v., & Berry, J. A. (1980). A biochemical model of photosynthetic CO2 assimilation in leaves of C3 species. *Planta*, *149*(1), 78-90.

Frankenberg, C., Fisher, J. B., Worden, J., Badgley, G., Saatchi, S. S., Lee, J. E., . . . Kuze, A. (2011). New global observations of the terrestrial carbon cycle from GOSAT: Patterns of plant fluorescence with gross primary productivity. *Geophysical Research Letters*, *38*(17).

Friedman, J. H. (2001). Greedy function approximation: a gradient boosting machine. *Annals of statistics*, 1189-1232.

Gardner, M. W., & Dorling, S. (1998). Artificial neural networks (the multilayer perceptron)—a review of applications in the atmospheric sciences. *Atmospheric environment, 32*(14-15), 2627-2636.

Greenwell, B. M., Boehmke, B. C., & McCarthy, A. J. (2018). A simple and effective model-based variable importance measure. *arXiv preprint arXiv:1805.04755*.

Groenendijk, M., Dolman, A., Van der Molen, M., Leuning, R., Arneth, A., Delpierre, N., . . . Verbeeck, H. (2011). Assessing parameter variability in a photosynthesis model within and between plant functional types using global Fluxnet eddy covariance data. *Agricultural and Forest Meteorology, 151*(1), 22-38.

Guan, X., Chen, J. M., Shen, H., Xie, X., & Tan, J. (2022). Comparison of big-leaf and two-leaf light use efficiency models for GPP simulation after considering a radiation scalar. *Agricultural and Forest Meteorology, 313*, 108761.

Hansen, N., & Kern, S. (2004). *Evaluating the CMA evolution strategy on multimodal test functions.* Paper presented at the International Conference on Parallel Problem Solving from Nature.

He, M., Ju, W., Zhou, Y., Chen, J., He, H., Wang, S., . . . Li, Y. (2013). Development of a two-leaf light use efficiency model for improving the calculation of terrestrial gross primary productivity. *Agricultural and Forest Meteorology, 173*, 28-39.

Horn, J., & Schulz, K. (2011a). Identification of a general light use efficiency model for gross primary production. *Biogeosciences, 8*(4), 999.

Horn, J., & Schulz, K. (2011b). Spatial extrapolation of light use efficiency model parameters to predict gross primary production. *Journal of Advances in Modeling Earth Systems, 3*(4).

Huntzinger, D. N., Michalak, A. M., Schwalm, C., Ciais, P., King, A. W., Fang, Y., . . . Zhao, F. (2017). Uncertainty in the response of terrestrial carbon sink to environmental drivers undermines carbon-climate feedback predictions. *Scientific Reports, 7*(1), 4765. Retrieved from https://doi.org/10.1038/s41598-017-03818-2. doi:10.1038/s41598-017-03818-2

Jung, M., Reichstein, M., Margolis, H. A., Cescatti, A., Richardson, A. D., Arain, M. A., . . . Chen, J. (2011). Global patterns of land‐atmosphere fluxes of carbon dioxide, latent heat, and sensible heat derived from eddy covariance, satellite, and meteorological observations. *Journal of Geophysical Research: Biogeosciences, 116*(G3).

Kalliokoski, T., Makela, A., Fronzek, S., Minunno, F., & Peltoniemi, M. (2018). Decomposing sources of uncertainty in climate change projections of boreal forest primary production. *Agricultural and Forest Meteorology, 262*, 192-205. Retrieved from <Go to ISI>://WOS:000444659300018. doi:10.1016/j.agrformet.2018.06.030

Kingma, D. P., & Ba, J. (2014). Adam: A method for stochastic optimization. *arXiv preprint arXiv:1412.6980*.

Kuppel, S., Peylin, P., Chevallier, F., Bacour, C., Maignan, F., & Richardson, A. (2012). Constraining a global ecosystem model with multi-site eddy-covariance data. *Biogeosciences, 9*(10), 3757-3776.

Lundberg, S. M., & Lee, S.-I. (2017). *A Unified Approach to Interpreting Model Predictions.* Paper presented at the 31st Annual Conference on Neural Information Processing Systems (NIPS), Long Beach, CA.

Luo, Y., & Schuur, E. A. G. (2020). Model parameterization to represent processes at unresolved scales and changing properties of evolving systems. *Global change biology, 26*(3), 1109-1117. Retrieved from <Go to ISI>://WOS:000506663700001. doi:10.1111/gcb.14939

Mahadevan, P., Wofsy, S. C., Matross, D. M., Xiao, X., Dunn, A. L., Lin, J. C., . . . Gottlieb, E. W. (2008). A satellite‐based biosphere parameterization for net ecosystem CO2 exchange: Vegetation Photosynthesis and Respiration Model (VPRM). *Global Biogeochemical Cycles, 22*(2).

Mäkelä, A., Pulkkinen, M., Kolari, P., Lagergren, F., Berbigier, P., Lindroth, A., . . . Hari, P. (2008). Developing an empirical model of stand GPP with the LUE approach: analysis of eddy covariance data at five contrasting conifer sites in Europe. *Global Change Biology, 14*(1), 92-108.

Masson-Delmotte, V., Zhai, P., Pirani, A., Connors, S. L., Péan, C., Berger, S., . . . Gomis, M. (2021). Climate change 2021: the physical science basis. *Contribution of working group I to the sixth assessment report of the intergovernmental panel on climate change*, 2.

McCulloch, W. S., & Pitts, W. (1943). A logical calculus of the ideas immanent in nervous activity. *The bulletin of mathematical biophysics, 5*(4), 115-133.

Medlyn, B. E., Robinson, A. P., Clement, R., & McMurtrie, R. E. (2005). On the validation of models of forest CO2 exchange using eddy covariance data: some perils and pitfalls. *Tree Physiology, 25*(7), 839-857. Retrieved from https://doi.org/10.1093/treephys/25.7.839. doi:10.1093/treephys/25.7.839

Mengoli, G., Agusti-Panareda, A., Boussetta, S., Harrison, S. P., Trotta, C., & Prentice, I. C. (2022). Ecosystem Photosynthesis in Land-Surface Models: A First-Principles Approach Incorporating Acclimation. *Journal*

of Advances in Modeling Earth Systems, 14(1). Retrieved from <Go to ISI>://WOS:000751889900010. doi:10.1029/2021ms002767

Montavon, G., Binder, A., Lapuschkin, S., Samek, W., & Müller, K.-R. (2019). Layer-wise relevance propagation: an overview. *Explainable AI: interpreting, explaining and visualizing deep learning*, 193-209.

Monteith, J. (1972). Solar radiation and productivity in tropical ecosystems. *Journal of applied ecology, 9*(3), 747-766.

Peaucelle, M., Bacour, C., Ciais, P., Vuichard, N., Kuppel, S., Peñuelas, J., . . . Chen, J. (2019). Covariations between plant functional traits emerge from constraining parameterization of a terrestrial biosphere model. *Global Ecology and Biogeography, 28*(9), 1351-1365.

Pedregosa, F., Varoquaux, G., Gramfort, A., Michel, V., Thirion, B., Grisel, O., . . . Dubourg, V. (2011). Scikit-learn: Machine learning in Python. *the Journal of machine Learning research, 12*, 2825-2830.

Piao, S., Wang, X., Wang, K., Li, X., Bastos, A., Canadell, J. G., . . . Sitch, S. (2020). Interannual variation of terrestrial carbon cycle: Issues and perspectives. *Global Change Biology, 26*(1), 300-318.

Poggio, L., de Sousa, L. M., Batjes, N. H., Heuvelink, G. B. M., Kempen, B., Ribeiro, E., & Rossiter, D. (2021). SoilGrids 2.0: producing soil information for the globe with quantified spatial uncertainty. *SOIL, 7*(1), 217-240. Retrieved from https://soil.copernicus.org/articles/7/217/2021/. doi:10.5194/soil-7-217-2021

Potter, C. S., Randerson, J. T., Field, C. B., Matson, P. A., Vitousek, P. M., Mooney, H. A., & Klooster, S. A. (1993). Terrestrial ecosystem production: a process model based on global satellite and surface data. *Global Biogeochemical Cycles, 7*(4), 811-841.

Prentice, I. C., Dong, N., Gleason, S. M., Maire, V., & Wright, I. J. (2014). Balancing the costs of carbon gain and water transport: testing a new theoretical framework for plant functional ecology. *Ecology letters, 17*(1), 82-91.

Rubel, F., Brugger, K., Haslinger, K., & Auer, I. (2017). The climate of the European Alps: Shift of very high resolution Köppen-Geiger climate zones 1800–2100. *Meteorologische Zeitschrift, 26*(2), 115-125.

Running, S. W., Nemani, R. R., Heinsch, F. A., Zhao, M., Reeves, M., & Hashimoto, H. (2004). A continuous satellite-derived measure of global terrestrial primary production. *Bioscience, 54*(6), 547-560.

Ryu, Y., Berry, J. A., & Baldocchi, D. D. (2019). What is global photosynthesis? History, uncertainties and opportunities. *Remote Sensing of Environment, 223*, 95-114. Retrieved from https://www.sciencedirect.com/science/article/pii/S0034425719300161. doi:https://doi.org/10.1016/j.rse.2019.01.016

Srivastava, N., Hinton, G., Krizhevsky, A., Sutskever, I., & Salakhutdinov, R. (2014). Dropout: A Simple Way to Prevent Neural Networks from Overfitting. *Journal of Machine Learning Research, 15*, 1929-1958. Retrieved from <Go to ISI>://WOS:000344638300002.

Stocker, B. D., Wang, H., Smith, N. G., Harrison, S. P., Keenan, T. F., Sandoval, D., . . . Prentice, I. C. (2020). P-model v1. 0: an optimality-based light use efficiency model for simulating ecosystem gross primary production. *Geoscientific Model Development, 13*(3), 1545-1581.

Stocker, T. (2014). *Climate change 2013: the physical science basis: Working Group I contribution to the Fifth assessment report of the Intergovernmental Panel on Climate Change*: Cambridge university press.

Tian, X., Minunno, F., Cao, T., Peltoniemi, M., Kalliokoski, T., & Mäkelä, A. (2020). Extending the range of applicability of the semi‐empirical ecosystem flux model PRELES for varying forest types and climate. *Global Change Biology, 26*(5), 2923-2943.

Wang, H., Prentice, I. C., Keenan, T. F., Davis, T. W., Wright, I. J., Cornwell, W. K., . . . Peng, C. (2017). Towards a universal model for carbon dioxide uptake by plants. *Nature Plants, 3*(9), 734-741.

Wang, R., Goll, D., Balkanski, Y., Hauglustaine, D., Boucher, O., Ciais, P., . . . Sardans, J. (2017). Global forest carbon uptake due to nitrogen and phosphorus deposition from 1850 to 2100. *Global Change Biology, 23*(11), 4854-4872.

Wenzel, S., Cox, P. M., Eyring, V., & Friedlingstein, P. (2014). Emergent constraints on climate‐carbon cycle feedbacks in the CMIP5 Earth system models. *Journal of Geophysical Research: Biogeosciences, 119*(5), 794-807.

Xiao, X., Hollinger, D., Aber, J., Goltz, M., Davidson, E. A., Zhang, Q., & Moore III, B. (2004). Satellite-based modeling of gross primary production in an evergreen needleleaf forest. *Remote Sensing of Environment, 89*(4), 519-534.

Xie, X., & Li, A. (2020). An adjusted two‐leaf light use efficiency model for improving GPP simulations over mountainous areas. *Journal of Geophysical Research: Atmospheres, 125*(13), e2019JD031702.

Xu, T., & Hutchinson, M. (2011). ANUCLIM version 6.1 user guide. *The Australian National University, Fenner School of Environment and Society, Canberra, 90*.

Yan, H., Wang, S. Q., Yu, K. L., Wang, B., Yu, Q., Bohrer, G., . . . Shugart, H. H. (2017). A Novel Diffuse Fraction ‐ Based Two ‐ Leaf Light Use Efficiency Model: An Application Quantifying Photosynthetic Seasonality across 20 AmeriFlux Flux Tower Sites. *Journal of Advances in Modeling Earth Systems, 9*(6), 2317-2332.

Yuan, W., Cai, W., Liu, S., Dong, W., Chen, J., Arain, M. A., . . . Georgiadis, T. (2014). Vegetation-specific model parameters are not required for estimating gross primary production. *Ecological Modelling, 292*, 1-10.

Yuan, W., Cai, W., Xia, J., Chen, J., Liu, S., Dong, W., . . . Beringer, J. (2014). Global comparison of light use efficiency models for simulating terrestrial vegetation gross primary production based on the LaThuile database. *Agricultural and Forest Meteorology, 192*, 108-120.

Yuan, W., Liu, S., Zhou, G., Zhou, G., Tieszen, L. L., Baldocchi, D., . . . Goulden, M. L. (2007). Deriving a light use efficiency model from eddy covariance flux data for predicting daily gross primary production across biomes. *Agricultural and Forest Meteorology, 143*(3-4), 189-207.

Yuan, W., Zheng, Y., Piao, S., Ciais, P., Lombardozzi, D., Wang, Y., . . . Hu, Z. (2019). Increased atmospheric vapor pressure deficit reduces global vegetation growth. *Science advances, 5*(8), eaax1396.

Zhang, F., Chen, J. M., Chen, J., Gough, C. M., Martin, T. A., & Dragoni, D. (2012). Evaluating spatial and temporal patterns of MODIS GPP over the conterminous US against flux measurements and a process model. *Remote Sensing of Environment, 124*, 717-729.

Zheng, Y., Shen, R., Wang, Y., Li, X., Liu, S., Liang, S., . . . Yuan, W. (2020). Improved estimate of global gross primary production for reproducing its long-term variation, 1982–2017. *Earth System Science Data, 12*(4), 2725-2746.

Zheng, Y., Zhang, L., Xiao, J., Yuan, W., Yan, M., Li, T., & Zhang, Z. (2018). Sources of uncertainty in gross primary productivity simulated by light use efficiency models: Model structure, parameters, input data, and spatial resolution. *Agricultural and Forest Meteorology, 263*, 242-257. Retrieved from http://www.sciencedirect.com/science/article/pii/S0168192318302636. doi:https://doi.org/10.1016/j.agrformet.2018.08.003

Zhou, Y., Wu, X., Ju, W., Chen, J. M., Wang, S., Wang, H., . . . Ibrom, A. (2016). Global parameterization and validation of a two ‐ leaf light use efficiency model for predicting gross primary production across FLUXNET sites. *Journal of Geophysical Research: Biogeosciences, 121*(4), 1045-1072.

References From the Supporting Information

Acosta, M., Pavelka, M., Montagnani, L., Kutsch, W., Lindroth, A., Juszczak, R., & Janouš, D. (2013). Soil surface CO2 efflux measurements in Norway spruce forests: Comparison between four different sites across Europe — from boreal to alpine forest. *Geoderma, 192*, 295-303. doi:https://doi.org/10.1016/j.geoderma.2012.08.027

Ammann, C., Spirig, C., Leifeld, J., & Neftel, A. (2009). Assessment of the nitrogen and carbon budget of two managed temperate grassland fields. *Agriculture, Ecosystems & Environment, 133*(3), 150-162. doi:https://doi.org/10.1016/j.agee.2009.05.006

Anthoni, P. M., Knohl, A., Rebmann, C., Freibauer, A., Mund, M., Ziegler, W., Kolle, O., & Schulze, E.-D. (2004a). Forest and agricultural land-use-dependent CO2 exchange in Thuringia, Germany. *Global change biology, 10*(12), 2005-2019. doi:https://doi.org/10.1111/j.1365-2486.2004.00863.x

Anthoni, P. M., Knohl, A., Rebmann, C., Freibauer, A., Mund, M., Ziegler, W., Kolle, O., & Schulze, E. D. (2004b). Forest and agricultural land ‐ use ‐ dependent CO2 exchange in Thuringia, Germany. *Global change biology, 10*(12), 2005-2019. doi:10.1111/J.1365-2486.2004.00863.X

Arain, M. A., & Restrepo-Coupe, N. (2005). Net ecosystem production in a temperate pine plantation in southeastern Canada. *Agricultural and Forest Meteorology, 128*(3-4), 223-241.

Archibald, S. A., Kirton, A., van der Merwe, M. R., Scholes, R. J., Williams, C. A., & Hanan, N. (2009). Drivers of inter-annual variability in Net Ecosystem Exchange in a semi-arid savanna ecosystem, South Africa. *Biogeosciences, 6*(2), 251-266. doi:10.5194/bg-6-251-2009

Ardö, J., Mölder, M., El-Tahir, B. A., & Elkhidir, H. A. M. (2008). Seasonal variation of carbon fluxes in a sparse savanna in semi arid Sudan. *Carbon Balance and Management, 3*(1), 7. doi:10.1186/1750-0680-3-7

Arneth, A., Kurbatova, J., Kolle, O., Shibistova, O. B., Lloyd, J., Vygodskaya, N. N., & Schulze, E. D. (2002). Comparative ecosystem–atmosphere exchange of energy and mass in a European Russian and a central

Siberian bog II. Interseasonal and interannual variability of CO2 fluxes. *Tellus B: Chemical and Physical Meteorology, 54*(5), 514-530. doi:10.3402/tellusb.v54i5.16684

Aubinet, M., Moureaux, C., Bodson, B., Dufranne, D., Heinesch, B., Suleau, M., Vancutsem, F., & Vilret, A. (2009). Carbon sequestration by a crop over a 4-year sugar beet/winter wheat/seed potato/winter wheat rotation cycle. *Agricultural and Forest Meteorology, 149*(3-4), 407-418.

Aurela, M., Lohila, A., Tuovinen, J. P., Hatakka, J., Penttila, T., & Laurila, T. (2015). Carbon dioxide and energy flux measurements in four northern-boreal ecosystems at Pallas. *Boreal Environment Research, 20*(4), 455-473.

AURELA, M., RIUTTA, T., LAURILA, T., TUOVINEN, J.-P., VESALA, T., TUITTILA, E.-S., RINNE, J., HAAPANALA, S., & LAINE, J. (2007). CO2 exchange of a sedge fen in southern Finland—the impact of a drought period. *Tellus B, 59*(5), 826-837. doi:https://doi.org/10.1111/j.1600-0889.2007.00309.x

Baldocchi, D. D., Vogel, C. A., & Hall, B. (1997). Seasonal variation of carbon dioxide exchange rates above and below a boreal jack pine forest. *Agricultural and Forest Meteorology, 83*(1-2), 147-170.

Bao, S., Wutzler, T., Koirala, S., Cuntz, M., Ibrom, A., Besnard, S., Walther, S., Šigut, L., Moreno, A., & Weber, U. (2022). Environment-sensitivity functions for gross primary productivity in light use efficiency models. *Agricultural and Forest Meteorology, 312*, 108708.

Belelli Marchesini, L., Papale, D., Reichstein, M., Vuichard, N., Tchebakova, N., & Valentini, R. (2007). Carbon balance assessment of a natural steppe of southern Siberia by multiple constraint approach. *Biogeosciences, 4*(4), 581-595. doi:10.5194/bg-4-581-2007

Berbigier, P., Bonnefond, J.-M., & Mellmann, P. (2001). CO2 and water vapour fluxes for 2 years above Euroflux forest site. *Agricultural and Forest Meteorology, 108*(3), 183-197. doi:https://doi.org/10.1016/S0168-1923(01)00240-4

Bergeron, O., Margolis, H. A., Black, T. A., Coursolle, C., Dunn, A. L., Barr, A. G., & Wofsy, S. C. (2007). Comparison of carbon dioxide fluxes over three boreal black spruce forests in Canada. *Global change biology, 13*(1), 89-107.

Beringer, J., Hacker, J., Hutley, L. B., Leuning, R., Arndt, S. K., Amiri, R., Bannehr, L., Cernusak, L. A., Grover, S., & Hensley, C. (2011). SPECIAL—Savanna patterns of energy and carbon integrated across the landscape. *Bulletin of the American Meteorological Society, 92*(11), 1467-1485.

Beringer, J., Hutley, L. B., McHugh, I., Arndt, S. K., Campbell, D., Cleugh, H. A., Cleverly, J., Resco de Dios, V., Eamus, D., & Evans, B. (2016). An introduction to the Australian and New Zealand flux tower network–OzFlux. *Biogeosciences, 13*(21), 5895-5916.

Beringer, J., Hutley, L. B., Tapper, N. J., Coutts, A., Kerley, A., & O'Grady, A. P. (2003). Fire impacts on surface heat, moisture and carbon fluxes from a tropical savanna in northern Australia. *International Journal of Wildland Fire, 12*(4), 333-340.

Bernhofer, C., Aubinet, M., Clement, R., Grelle, A., Grünwald, T., Ibrom, A., Jarvis, P., Rebmann, C., Schulze, E.-D., & Tenhunen, J. D. (2003). Spruce Forests (Norway and Sitka Spruce, Including Douglas Fir): Carbon and Water Fluxes and Balances, Ecological and Ecophysiological Determinants. In R. Valentini (Ed.), *Fluxes of Carbon, Water and Energy of European Forests* (pp. 99-123). Berlin, Heidelberg: Springer Berlin Heidelberg.

Besnard, S., Carvalhais, N., Arain, M. A., Black, A., Brede, B., Buchmann, N., Chen, J., Clevers, J. G. W., Dutrieux, L. P., & Gans, F. (2019). Memory effects of climate and vegetation affecting net ecosystem CO2 fluxes in global forests. *Plos One, 14*(2), e0211510.

Billesbach D, B. J., Torn M. (2016). *FLUXNET2015 US-AR1 ARM USDA UNL OSU Woodward Switchgrass 1*. Retrieved from FluxNet; Lawerence Berkeley National Lab; US Department of Agriculture; Univ. of Nebraska, Lincoln, NE (United States):

Black, T., Den Hartog, G., Neumann, H., Blanken, P., Yang, P., Russell, C., Nesic, Z., Lee, X., Chen, S., & Staebler, R. (1996). Annual cycles of water vapour and carbon dioxide fluxes in and above a boreal aspen forest. *Global change biology, 2*(3), 219-229.

Bloom, A., & Williams, M. (2015). Constraining ecosystem carbon dynamics in a data-limited world: integrating ecological" common sense" in a model–data fusion framework. *Biogeosciences, 12*(5), 1299-1315.

Bloomfield, K. J., Cernusak, L. A., Eamus, D., Ellsworth, D. S., Colin Prentice, I., Wright, I. J., Boer, M. M., Bradford, M. G., Cale, P., & Cleverly, J. (2018). A continental ‐ scale assessment of variability in leaf traits: Within species, across sites and between seasons. *Functional Ecology, 32*(6), 1492-1506.

Boese, S., Jung, M., Carvalhais, N., Teuling, A. J., & Reichstein, M. (2019). Carbon–water flux coupling under progressive drought. *Biogeosciences, 16*(13), 2557-2572.

Bristow, M., Hutley, L. B., Beringer, J., Livesley, S. J., Edwards, A. C., & Arndt, S. K. (2016). Quantifying the relative importance of greenhouse gas emissions from current and future savanna land use change across northern Australia. *Biogeosciences, 13*(22), 6285-6303.

Carrara, A., Janssens, I. A., Yuste, J. C., & Ceulemans, R. (2004). Seasonal changes in photosynthesis, respiration and NEE of a mixed temperate forest. *Agricultural and Forest Meteorology, 126*(1-2), 15-31.

Chen, S., Chen, J., Lin, G., Zhang, W., Miao, H., Wei, L., Huang, J., & Han, X. (2009). Energy balance and partition in Inner Mongolia steppe ecosystems with different land use types. *Agricultural and Forest Meteorology, 149*(11), 1800-1809. doi:https://doi.org/10.1016/j.agrformet.2009.06.009

Chiesi, M., Maselli, F., Bindi, M., Fibbi, L., Cherubini, P., Arlotta, E., Tirone, G., Matteucci, G., & Seufert, G. (2005). Modelling carbon budget of Mediterranean forests using ground and remote sensing measurements. *Agricultural and Forest Meteorology, 135*(1), 22-34. doi:https://doi.org/10.1016/j.agrformet.2005.09.011

Clark, K. L., Gholz, H. L., Moncrieff, J. B., Cropley, F., & Loescher, H. W. (1999). ENVIRONMENTAL CONTROLS OVER NET EXCHANGES OF CARBON DIOXIDE FROM CONTRASTING FLORIDA ECOSYSTEMS. *Ecological Applications, 9*(3), 936-948. doi:https://doi.org/10.1890/1051-0761(1999)009[0936:ECONEO]2.0.CO;2

Cleverly, J., Boulain, N., Villalobos‐Vega, R., Grant, N., Faux, R., Wood, C., Cook, P. G., Yu, Q., Leigh, A., & Eamus, D. (2013). Dynamics of component carbon fluxes in a semi‐arid Acacia woodland, central Australia. *Journal of Geophysical Research: Biogeosciences, 118*(3), 1168-1185.

Cleverly, J., Eamus, D., Van Gorsel, E., Chen, C., Rumman, R., Luo, Q., Coupe, N. R., Li, L., Kljun, N., Faux, R., Yu, Q., & Huete, A. (2016). Productivity and evapotranspiration of two contrasting semiarid ecosystems following the 2011 global carbon land sink anomaly. *Agricultural and Forest Meteorology, 220*, 151-159. doi:https://doi.org/10.1016/j.agrformet.2016.01.086

Cook, B. D., Davis, K. J., Wang, W., Desai, A., Berger, B. W., Teclaw, R. M., Martin, J. G., Bolstad, P. V., Bakwin, P. S., Yi, C., & Heilman, W. (2004). Carbon exchange and venting anomalies in an upland deciduous forest in northern Wisconsin, USA. *Agricultural and Forest Meteorology, 126*(3), 271-295. doi:https://doi.org/10.1016/j.agrformet.2004.06.008

Coursolle, C., Margolis, H., Giasson, M.-A., Bernier, P.-Y., Amiro, B., Arain, M., Barr, A., Black, T., Goulden, M., & McCaughey, J. (2012). Influence of stand age on the magnitude and seasonality of carbon fluxes in Canadian forests. *Agricultural and Forest Meteorology, 165*, 136-148.

D., B. (2016). *AmeriFlux US-Cop Corral Pocket*. Retrieved from Lawrence Berkeley National Lab.(LBNL), Berkeley, CA (United States). AmeriFlux; Univ. of Utah, Salt Lake City, UT (United States):

Da Rocha, H. R., Manzi, A. O., Cabral, O. M., Miller, S. D., Goulden, M. L., Saleska, S. R., R.‐Coupe, N., Wofsy, S. C., Borma, L. S., & Artaxo, P. (2009). Patterns of water and heat flux across a biome gradient from tropical forest to savanna in Brazil. *Journal of Geophysical Research: Biogeosciences, 114*(G1).

DeForest, J. L., Noormets, A., McNulty, S. G., Sun, G., Tenney, G., & Chen, J. (2006). Phenophases alter the soil respiration–temperature relationship in an oak-dominated forest. *International Journal of Biometeorology, 51*(2), 135-144. doi:10.1007/s00484-006-0046-7

Desai, A. R., Bolstad, P. V., Cook, B. D., Davis, K. J., & Carey, E. V. (2005). Comparing net ecosystem exchange of carbon dioxide between an old-growth and mature forest in the upper Midwest, USA. *Agricultural and Forest Meteorology, 128*(1), 33-55. doi:https://doi.org/10.1016/j.agrformet.2004.09.005

Dolman, A. J., Moors, E. J., & Elbers, J. A. (2002). The carbon uptake of a mid latitude pine forest growing on sandy soil. *Agricultural and Forest Meteorology, 111*(3), 157-170. doi:https://doi.org/10.1016/S0168-1923(02)00024-2

DON, A., REBMANN, C., KOLLE, O., SCHERER-LORENZEN, M., & SCHULZE, E.-D. (2009). Impact of afforestation-associated management changes on the carbon balance of grassland. *Global change biology, 15*(8), 1990-2002. doi:https://doi.org/10.1111/j.1365-2486.2009.01873.x

Dušek, J., Čížková, H., Stellner, S., Czerný, R., & Květ, J. (2012). Fluctuating water table affects gross ecosystem production and gross radiation use efficiency in a sedge-grass marsh. *Hydrobiologia, 692*(1), 57-66. doi:10.1007/s10750-012-0998-z

Epstein, H. E., Calef, M. P., Walker, M. D., Stuart Chapin III, F., & Starfield, A. M. (2004). Detecting changes in arctic tundra plant communities in response to warming over decadal time scales. *Global change biology, 10*(8), 1325-1334. doi:https://doi.org/10.1111/j.1529-8817.2003.00810.x

Ferréa, C., Zenone, T., Comolli, R., & Seufert, G. (2012). Estimating heterotrophic and autotrophic soil respiration in a semi-natural forest of Lombardy, Italy. *Pedobiologia, 55*(6), 285-294. doi:https://doi.org/10.1016/j.pedobi.2012.05.001

Flanagan, L. B., Wever, L. A., & Carlson, P. J. (2002). Seasonal and interannual variation in carbon dioxide exchange and carbon balance in a northern temperate grassland. *Global change biology, 8*(7), 599-615.

Flechard, C. R., Oijen, M. v., Cameron, D. R., Vries, W. d., Ibrom, A., Buchmann, N., Dise, N. B., Janssens, I. A., Neirynck, J., & Montagnani, L. (2020). Carbon–nitrogen interactions in European forests and semi-natural vegetation–Part 2: Untangling climatic, edaphic, management and nitrogen deposition effects on carbon sequestration potentials. *Biogeosciences, 17*(6), 1621-1654.

Fu, P., & Rich, P. M. (1999). *Design and implementation of the Solar Analyst: an ArcView extension for modeling solar radiation at landscape scales.* Paper presented at the Proceedings of the nineteenth annual ESRI user conference.

Galvagno, M., Wohlfahrt, G., Cremonese, E., Rossini, M., Colombo, R., Filippa, G., Julitta, T., Manca, G., Siniscalco, C., di Cella, U. M., & Migliavacca, M. (2013). Phenology and carbon dioxide source/sink strength of a subalpine grassland in response to an exceptionally short snow season. *Environmental Research Letters, 8*(2). doi:10.1088/1748-9326/8/2/025008

Giasson, M.-A., Coursolle, C., & Margolis, H. A. (2006). Ecosystem-level CO2 fluxes from a boreal cutover in eastern Canada before and after scarification. *Agricultural and Forest Meteorology, 140*(1-4), 23-40.

Gilmanov, T. G., Tieszen, L. L., Wylie, B. K., Flanagan, L. B., Frank, A. B., Haferkamp, M. R., Meyers, T. P., & Morgan, J. A. (2005). Integration of CO2 flux and remotely-sensed data for primary production and ecosystem respiration analyses in the Northern Great Plains: potential for quantitative spatial extrapolation. *Global ecology and biogeography, 14*(3), 271-292. doi:https://doi.org/10.1111/j.1466-822X.2005.00151.x

Goldstein, A. H., Hultman, N. E., Fracheboud, J. M., Bauer, M. R., Panek, J. A., Xu, M., Qi, Y., Guenther, A. B., & Baugh, W. (2000). Effects of climate variability on the carbon dioxide, water, and sensible heat fluxes above a ponderosa pine plantation in the Sierra Nevada (CA). *Agricultural and Forest Meteorology, 101*(2), 113-129. doi:https://doi.org/10.1016/S0168-1923(99)00168-9

Gough, C. M., Vogel, C. S., Schmid, H. P., Su, H. B., & Curtis, P. S. (2008). Multi-year convergence of biometric and meteorological estimates of forest carbon storage. *Agricultural and Forest Meteorology, 148*(2), 158-170. doi:https://doi.org/10.1016/j.agrformet.2007.08.004

Granier, A., Ceschia, E., Damesin, C., Dufrêne, E., Epron, D., Gross, P., Lebaube, S., Le Dantec, V., Le Goff, N., Lemoine, D., Lucot, E., Ottorini, J. M., Pontailler, J. Y., & Saugier, B. (2000). The carbon balance of a young Beech forest. *Functional Ecology, 14*(3), 312-325. doi:https://doi.org/10.1046/j.1365-2435.2000.00434.x

Griebel, A., Bennett, L. T., Metzen, D., Cleverly, J., Burba, G., & Arndt, S. K. (2016). Effects of inhomogeneities within the flux footprint on the interpretation of seasonal, annual, and interannual ecosystem carbon exchange. *Agricultural and Forest Meteorology, 221*, 50-60.

Gu, L., Pallardy, S. G., Yang, B., Hosman, K. P., Mao, J., Ricciuto, D., Shi, X., & Sun, Y. (2016). Testing a land model in ecosystem functional space via a comparison of observed and modeled ecosystem flux responses to precipitation regimes and associated stresses in a Central U.S. forest. *Journal of Geophysical Research: Biogeosciences, 121*(7), 1884-1902. doi:https://doi.org/10.1002/2015JG003302

Hansen, N., & Kern, S. (2004). *Evaluating the CMA evolution strategy on multimodal test functions.* Paper presented at the International conference on parallel problem solving from nature.

Hao, Y., Baik, J., & Choi, M. (2019). Developing a soil water index-based Priestley–Taylor algorithm for estimating evapotranspiration over East Asia and Australia. *Agricultural and Forest Meteorology, 279*, 107760.

Heinsch, F. A., Heilman, J. L., McInnes, K. J., Cobos, D. R., Zuberer, D. A., & Roelke, D. L. (2004). Carbon dioxide exchange in a high marsh on the Texas Gulf Coast: effects of freshwater availability. *Agricultural and Forest Meteorology, 125*(1), 159-172. doi:https://doi.org/10.1016/j.agrformet.2004.02.007

Henderson‐Sellers, B. (1984). A new formula for latent heat of vaporization of water as a function of temperature. *Quarterly Journal of the Royal Meteorological Society, 110*(466), 1186-1190.

Hollinger, D. Y., Goltz, S. M., Davidson, E. A., Lee, J. T., Tu, K., & Valentine, H. T. (1999). Seasonal patterns and environmental control of carbon dioxide and water vapour exchange in an ecotonal boreal forest. *Global change biology, 5*(8), 891-902. doi:https://doi.org/10.1046/j.1365-2486.1999.00281.x

Hommeltenberg, J., Schmid, H. P., Drösler, M., & Werle, P. (2014). Can a bog drained for forestry be a stronger carbon sink than a natural bog forest? *Biogeosciences, 11*(13), 3477-3493. doi:10.5194/bg-11-3477-2014

Howard, E. A., Gower, S. T., Foley, J. A., & Kucharik, C. J. (2004). Effects of logging on carbon dynamics of a jack pine forest in Saskatchewan, Canada. *Global change biology, 10*(8), 1267-1284.

Humphreys, E. R., Black, T. A., Morgenstern, K., Cai, T., Drewitt, G. B., Nesic, Z., & Trofymow, J. (2006). Carbon dioxide fluxes in coastal Douglas-fir stands at different stages of development after clearcut harvesting. *Agricultural and Forest Meteorology, 140*(1-4), 6-22.

Hutley, L. B., Beringer, J., Isaac, P. R., Hacker, J. M., & Cernusak, L. A. (2011). A sub-continental scale living laboratory: Spatial patterns of savanna vegetation over a rainfall gradient in northern Australia. *Agricultural and Forest Meteorology, 151*(11), 1417-1428.

Ikawa, H., Nakai, T., Busey, R. C., Kim, Y., Kobayashi, H., Nagai, S., Ueyama, M., Saito, K., Nagano, H., Suzuki, R., & Hinzman, L. (2015). Understory CO2, sensible heat, and latent heat fluxes in a black spruce forest in interior Alaska. *Agricultural and Forest Meteorology, 214-215*, 80-90. doi:https://doi.org/10.1016/j.agrformet.2015.08.247

Imer, D., Merbold, L., Eugster, W., & Buchmann, N. (2013). Temporal and spatial variations of soil CO₂, CH₄ and N₂O fluxes at three differently managed grasslands. *Biogeosciences, 10*(9), 5931-5945. doi:10.5194/bg-10-5931-2013

Jacobs, C. M. J., Jacobs, A. F. G., Bosveld, F. C., Hendriks, D. M. D., Hensen, A., Kroon, P. S., Moors, E. J., Nol, L., Schrier-Uijl, A., & Veenendaal, E. M. (2007). Variability of annual CO₂ exchange from Dutch grasslands. *Biogeosciences, 4*(5), 803-816. doi:10.5194/bg-4-803-2007

Jarvis, P., Massheder, J., Hale, S., Moncrieff, J., Rayment, M., & Scott, S. (1997). Seasonal variation of carbon dioxide, water vapor, and energy exchanges of a boreal black spruce forest. *Journal of Geophysical Research: Atmospheres, 102*(D24), 28953-28966.

Knohl, A., Schulze, E.-D., Kolle, O., & Buchmann, N. (2003). Large carbon uptake by an unmanaged 250-year-old deciduous forest in Central Germany. *Agricultural and Forest Meteorology, 118*(3), 151-167. doi:https://doi.org/10.1016/S0168-1923(03)00115-1

Koskinen, M., Minkkinen, K., Ojanen, P., Kämäräinen, M., Laurila, T., & Lohila, A. (2014). Measurements of CO₂ exchange with an automated chamber system throughout the year: challenges in measuring night-time respiration on porous peat soil. *Biogeosciences, 11*(2), 347-363. doi:10.5194/bg-11-347-2014

Krupková, L., Marková, I., Havránková, K., Pokorný, R., Urban, O., Šigut, L., Pavelka, M., Cienciala, E., & Marek, M. V. (2017). Comparison of different approaches of radiation use efficiency of biomass formation estimation in Mountain Norway spruce. *Trees, 31*(1), 325-337. doi:10.1007/s00468-016-1486-2

Kurbatova, J., Li, C., Varlagin, A., Xiao, X., & Vygodskaya, N. (2008). Modeling carbon dynamics in two adjacent spruce forests with different soil conditions in Russia. *Biogeosciences, 5*(4), 969-980. doi:10.5194/bg-5-969-2008

Kwon, H., Law, B. E., Thomas, C. K., & Johnson, B. G. (2018). The influence of hydrological variability on inherent water use efficiency in forests of contrasting composition, age, and precipitation regimes in the Pacific Northwest. *Agricultural and Forest Meteorology, 249*, 488-500. doi:https://doi.org/10.1016/j.agrformet.2017.08.006

Lafleur, P. M., Roulet, N. T., Bubier, J. L., Frolking, S., & Moore, T. R. (2003). Interannual variability in the peatland - atmosphere carbon dioxide exchange at an ombrotrophic bog. *Global Biogeochemical Cycles, 17*(2).

Law, B. E., Thornton, P. E., Irvine, J., Anthoni, P. M., & Van Tuyl, S. (2001). Carbon storage and fluxes in ponderosa pine forests at different developmental stages. *Global change biology, 7*(7), 755-777. doi:https://doi.org/10.1046/j.1354-1013.2001.00439.x

Leuning, R., Cleugh, H. A., Zegelin, S. J., & Hughes, D. (2005). Carbon and water fluxes over a temperate Eucalyptus forest and a tropical wet/dry savanna in Australia: measurements and comparison with MODIS remote sensing estimates. *Agricultural and Forest Meteorology, 129*(3-4), 151-173.

Lipson, D. A., Wilson, R. F., & Oechel, W. C. (2005). Effects of Elevated Atmospheric CO₂ on Soil Microbial Biomass, Activity, and Diversity in a Chaparral Ecosystem. *Applied and Environmental Microbiology, 71*(12), 8573-8580. doi:10.1128/aem.71.12.8573-8580.2005

López-Ballesteros, A., Serrano-Ortiz, P., Kowalski, A. S., Sánchez-Cañete, E. P., Scott, R. L., & Domingo, F. (2017). Subterranean ventilation of allochthonous CO2 governs net CO2 exchange in a semiarid Mediterranean grassland. *Agricultural and Forest Meteorology, 234-235*, 115-126. doi:https://doi.org/10.1016/j.agrformet.2016.12.021

Loubet, B., Laville, P., Lehuger, S., Larmanou, E., Flechard, C., Mascher, N., Genermont, S., Roche, R., Ferrara, R. M., Stella, P., Personne, E., Durand, B., Decuq, C., Flura, D., Masson, S., Fanucci, O., Rampon, J. N., Siemens, J., Kindler, R., Gabrielle, B., et al. (2011). Carbon, nitrogen and Greenhouse gases budgets over a four years crop rotation in northern France. *Plant and Soil, 343*(1-2), 109-137. doi:10.1007/s11104-011-0751-9

Lund, M., Falk, J. M., Friborg, T., Mbufong, H. N., Sigsgaard, C., Soegaard, H., & Tamstorf, M. P. (2012). Trends in CO2 exchange in a high Arctic tundra heath, 2000–2010. *Journal of Geophysical Research: Biogeosciences, 117*(G2). doi:https://doi.org/10.1029/2011JG001901

Ma, S., Baldocchi, D., Wolf, S., & Verfaillie, J. (2016). Slow ecosystem responses conditionally regulate annual carbon balance over 15 years in Californian oak-grass savanna. *Agricultural and Forest Meteorology, 228-229*, 252-264. doi:https://doi.org/10.1016/j.agrformet.2016.07.016

Ma, S., Baldocchi, D. D., Mambelli, S., & Dawson, T. E. (2011). Are temporal variations of leaf traits responsible for seasonal and inter-annual variability in ecosystem CO2 exchange? *Functional Ecology, 25*(1), 258-270. doi:https://doi.org/10.1111/j.1365-2435.2010.01779.x

Marcolla, B., Cescatti, A., Montagnani, L., Manca, G., Kerschbaumer, G., & Minerbi, S. (2005). Importance of advection in the atmospheric CO2 exchanges of an alpine forest. *Agricultural and Forest Meteorology, 130*(3), 193-206. doi:https://doi.org/10.1016/j.agrformet.2005.03.006

Marcolla, B., Pitacco, A., & Cescatti, A. (2003). Canopy Architecture and Turbulence Structure in a Coniferous Forest. *Boundary-Layer Meteorology, 108*(1), 39-59. doi:10.1023/A:1023027709805

Merbold, L., Ardö, J., Arneth, A., Scholes, R. J., Nouvellon, Y., de Grandcourt, A., Archibald, S., Bonnefond, J. M., Boulain, N., Brueggemann, N., Bruemmer, C., Cappelaere, B., Ceschia, E., El-Khidir, H. A. M., El-Tahir, B. A., Falk, U., Lloyd, J., Kergoat, L., Le Dantec, V., Mougin, E., et al. (2009). Precipitation as driver of carbon fluxes in 11 African ecosystems. *Biogeosciences, 6*(6), 1027-1041. doi:10.5194/bg-6-1027-2009

Merbold, L., Eugster, W., Stieger, J., Zahniser, M., Nelson, D., & Buchmann, N. (2014). Greenhouse gas budget (CO 2, CH 4 and N2O) of intensively managed grassland following restoration. *Global change biology, 20*(6), 1913-1928.

Meyer, W., Kondrlovà, E., & Koerber, G. (2015). Evaporation of perennial semi‐arid woodland in southeastern Australia is adapted for irregular but common dry periods. *Hydrological Processes, 29*(17), 3714-3726.

Michelot, A., Eglin, T., Dufrene, E., Lelarge-Trouverie, C., & Damesin, C. (2011). Comparison of seasonal variations in water-use efficiency calculated from the carbon isotope composition of tree rings and flux data in a temperate forest. *Plant Cell and Environment, 34*(2), 230-244. doi:10.1111/j.1365-3040.2010.02238.x

Migliavacca, M., Meroni, M., Manca, G., Matteucci, G., Montagnani, L., Grassi, G., Zenone, T., Teobaldelli, M., Goded, I., Colombo, R., & Seufert, G. (2009). Seasonal and interannual patterns of carbon and water fluxes of a poplar plantation under peculiar eco-climatic conditions. *Agricultural and Forest Meteorology, 149*(9), 1460-1476. doi:https://doi.org/10.1016/j.agrformet.2009.04.003

Mkhabela, M., Amiro, B., Barr, A., Black, T., Hawthorne, I., Kidston, J., McCaughey, J., Orchansky, A., Nesic, Z., & Sass, A. (2009). Comparison of carbon dynamics and water use efficiency following fire and harvesting in Canadian boreal forests. *Agricultural and Forest Meteorology, 149*(5), 783-794.

Monson, R. K., Turnipseed, A. A., Sparks, J. P., Harley, P. C., Scott-Denton, L. E., Sparks, K., & Huxman, T. E. (2002). Carbon sequestration in a high-elevation, subalpine forest. *Global change biology, 8*(5), 459-478. doi:https://doi.org/10.1046/j.1365-2486.2002.00480.x

Myneni, R. B., Ramakrishna, R., Nemani, R., & Running, S. W. (1997). Estimation of global leaf area index and absorbed PAR using radiative transfer models. *IEEE Transactions on Geoscience and Remote Sensing, 35*(6), 1380-1393.

Nakai, T., Kim, Y., Busey, R. C., Suzuki, R., Nagai, S., Kobayashi, H., Park, H., Sugiura, K., & Ito, A. (2013). Characteristics of evapotranspiration from a permafrost black spruce forest in interior Alaska. *Polar Science, 7*(2), 136-148. doi:https://doi.org/10.1016/j.polar.2013.03.003

Nardino, M., Georgiadis, T., Rossi, F., Ponti, F., Miglietta, F. & Magliulo, V. (2002). *Primary productivity and evapotranspiration of a mixed forest*. Paper presented at the Congress CNR-ISA Fo., Istituto per i Sistemi Agricoli e Forestali del Mediterraneo, Portici.

Noormets, A., Chen, J., & Crow, T. R. (2007). Age-Dependent Changes in Ecosystem Carbon Fluxes in Managed Forests in Northern Wisconsin, USA. *Ecosystems, 10*(2), 187-203. doi:10.1007/s10021-007-9018-y

Noormets, A., McNulty, S. G., Domec, J.-C., Gavazzi, M., Sun, G., & King, J. S. (2012). The role of harvest residue in rotation cycle carbon balance in loblolly pine plantations. Respiration partitioning approach. *Global change biology, 18*(10), 3186-3201. doi:https://doi.org/10.1111/j.1365-2486.2012.02776.x

Nossent, J., & Bauwens, W. (2012). *Application of a normalized Nash-Sutcliffe efficiency to improve the accuracy of the Sobol'sensitivity analysis of a hydrological model.* Paper presented at the EGU General Assembly Conference Abstracts.

Ouimette, A. P., Ollinger, S. V., Richardson, A. D., Hollinger, D. Y., Keenan, T. F., Lepine, L. C., & Vadeboncoeur, M. A. (2018). Carbon fluxes and interannual drivers in a temperate forest ecosystem assessed through

comparison of top-down and bottom-up approaches. *Agricultural and Forest Meteorology, 256-257*, 420-430. doi:https://doi.org/10.1016/j.agrformet.2018.03.017

Papale, D., Migliavacca, M., Cremonese, E., Cescatti, A., Alberti, G., Balzarolo, M., Belelli Marchesini, L., Canfora, E., Casa, R., Duce, P., Facini, O., Galvagno, M., Genesio, L., Gianelle, D., Magliulo, V., Matteucci, G., Montagnani, L., Petrella, F., Pitacco, A., Seufert, G., et al. (2015). Carbon, Water and Energy Fluxes of Terrestrial Ecosystems in Italy. In R. Valentini & F. Miglietta (Eds.), *The Greenhouse Gas Balance of Italy: An Insight on Managed and Natural Terrestrial Ecosystems* (pp. 11-45). Berlin, Heidelberg: Springer Berlin Heidelberg.

Pastorello, G., Trotta, C., Canfora, E., Chu, H., Christianson, D., Cheah, Y.-W., Poindexter, C., Chen, J., Elbashandy, A., & Humphrey, M. (2020). The FLUXNET2015 dataset and the ONEFlux processing pipeline for eddy covariance data. *Scientific data, 7*(1), 1-27.

Peichl, M., & Arain, M. A. (2007). Allometry and partitioning of above-and belowground tree biomass in an age-sequence of white pine forests. *Forest Ecology and Management, 253*(1-3), 68-80.

Pejam, M., Arain, M., & McCaughey, J. (2006). Energy and water vapour exchanges over a mixedwood boreal forest in Ontario, Canada. *Hydrological Processes, 20*(17), 3709-3724.

Pereira, J. S., Mateus, J. A., Aires, L. M., Pita, G., Pio, C., David, J. S., Andrade, V., Banza, J., David, T. S., Paço, T. A., & Rodrigues, A. (2007). Net ecosystem carbon exchange in three contrasting Mediterranean ecosystems – the effect of drought. *Biogeosciences, 4*(5), 791-802. doi:10.5194/bg-4-791-2007

Perez-Priego, O., El-Madany, T. S., Migliavacca, M., Kowalski, A. S., Jung, M., Carrara, A., Kolle, O., Martín, M. P., Pacheco-Labrador, J., Moreno, G., & Reichstein, M. (2017). Evaluation of eddy covariance latent heat fluxes with independent lysimeter and sapflow estimates in a Mediterranean savannah ecosystem. *Agricultural and Forest Meteorology, 236*, 87-99. doi:https://doi.org/10.1016/j.agrformet.2017.01.009

Pilegaard, K., & Ibrom, A. (2020). Net carbon ecosystem exchange during 24 years in the Sorø Beech Forest–relations to phenology and climate. *Tellus B: Chemical and Physical Meteorology, 72*(1), 1-17.

Poggio, L., de Sousa, L. M., Batjes, N. H., Heuvelink, G. B. M., Kempen, B., Ribeiro, E., & Rossiter, D. (2021). SoilGrids 2.0: producing soil information for the globe with quantified spatial uncertainty. *SOIL, 7*(1), 217-240. doi:10.5194/soil-7-217-2021

Powell, T. L., Bracho, R., Li, J., Dore, S., Hinkle, C. R., & Drake, B. G. (2006). Environmental controls over net ecosystem carbon exchange of scrub oak in central Florida. *Agricultural and Forest Meteorology, 141*(1), 19-34. doi:https://doi.org/10.1016/j.agrformet.2006.09.002

Prescher, A.-K., Grünwald, T., & Bernhofer, C. (2010). Land use regulates carbon budgets in eastern Germany: From NEE to NBP. *Agricultural and Forest Meteorology, 150*(7), 1016-1025. doi:10.1016/J.AGRFORMET.2010.03.008

Priestley, C. H. B., & Taylor, R. (1972). On the assessment of surface heat flux and evaporation using large-scale parameters. *Monthly weather review, 100*(2), 81-92.

Rambal, S., Joffre, R., Ourcival, J. M., Cavender-Bares, J., & Rocheteau, A. (2004). The growth respiration component in eddy CO2 flux from a Quercus ilex mediterranean forest. *Global change biology, 10*(9), 1460-1469. doi:https://doi.org/10.1111/j.1365-2486.2004.00819.x

Rebmann, C., Zeri, M., Lasslop, G., Mund, M., Kolle, O., Schulze, E.-D., & Feigenwinter, C. (2010). Treatment and assessment of the CO2-exchange at a complex forest site in Thuringia, Germany. *Agricultural and Forest Meteorology, 150*(5), 684-691. doi:https://doi.org/10.1016/j.agrformet.2009.11.001

Reichstein, M., Falge, E., Baldocchi, D., Papale, D., Aubinet, M., Berbigier, P., Bernhofer, C., Buchmann, N., Gilmanov, T., & Granier, A. (2005). On the separation of net ecosystem exchange into assimilation and ecosystem respiration: review and improved algorithm. *Global change biology, 11*(9), 1424-1439.

Renchon, A. A., Griebel, A., Metzen, D., Williams, C. A., Medlyn, B., Duursma, R. A., Barton, C. V., Maier, C., Boer, M. M., & Isaac, P. (2018). Upside-down fluxes Down Under: CO 2 net sink in winter and net source in summer in a temperate evergreen broadleaf forest. *Biogeosciences, 15*(12), 3703-3716.

Reverter, B. R., Sánchez-Cañete, E. P., Resco, V., Serrano-Ortiz, P., Oyonarte, C., & Kowalski, A. S. (2010). Analyzing the major drivers of NEE in a Mediterranean alpine shrubland. *Biogeosciences, 7*(9), 2601-2611. doi:10.5194/bg-7-2601-2010

Rey, A., Pegoraro, E., Tedeschi, V., De Parri, I., Jarvis, P. G., & Valentini, R. (2002). Annual variation in soil respiration and its components in a coppice oak forest in Central Italy. *Global change biology, 8*(9), 851-866. doi:https://doi.org/10.1046/j.1365-2486.2002.00521.x

Rodrigues, A., Pita, G., Mateus, J., Kurz-Besson, C., Casquilho, M., Cerasoli, S., Gomes, A., & Pereira, J. (2011). Eight years of continuous carbon fluxes measurements in a Portuguese eucalypt stand under two main

events: Drought and felling. *Agricultural and Forest Meteorology*, *151*(4), 493-507. doi:https://doi.org/10.1016/j.agrformet.2010.12.007

Roman, D. T., Novick, K. A., Brzostek, E. R., Dragoni, D., Rahman, F., & Phillips, R. P. (2015). The role of isohydric and anisohydric species in determining ecosystem-scale response to severe drought. *Oecologia, 179*(3), 641-654. doi:10.1007/s00442-015-3380-9

Rouse, J. W., Haas, R. H., Schell, J. A., Deering, D. W., & Harlan, J. C. (1974). Monitoring the vernal advancement and retrogradation (green wave effect) of natural vegetation. *NASA/GSFC Type III Final Report, Greenbelt, Md, 371*.

Rubel, F., Brugger, K., Haslinger, K., & Auer, I. (2017). The climate of the European Alps: Shift of very high resolution Köppen-Geiger climate zones 1800–2100. *Meteorologische Zeitschrift, 26*(2), 115-125.

Ruehr, N. K., Law, B. E., Quandt, D., & Williams, M. (2014). Effects of heat and drought on carbon and water dynamics in a regenerating semi-arid pine forest: a combined experimental and modeling approach. *Biogeosciences, 11*(15), 4139-4156. doi:10.5194/bg-11-4139-2014

Running, S. W., & Zhao, M. (2015). Daily GPP and annual NPP (MOD17A2/A3) products NASA Earth Observing System MODIS land algorithm. *MOD17 User's Guide, 2015*.

Sabbatini, S., Arriga, N., Bertolini, T., Castaldi, S., Chiti, T., Consalvo, C., Njakou Djomo, S., Gioli, B., Matteucci, G., & Papale, D. (2016). Greenhouse gas balance of cropland conversion to bioenergy poplar short-rotation coppice. *Biogeosciences, 13*(1), 95-113. doi:10.5194/bg-13-95-2016

Sagerfors, J., Lindroth, A., Grelle, A., Klemedtsson, L., Weslien, P., & Nilsson, M. (2008). Annual CO2 exchange between a nutrient-poor, minerotrophic, boreal mire and the atmosphere. *Journal of Geophysical Research: Biogeosciences, 113*(G1). doi:https://doi.org/10.1029/2006JG000306

Sanz M J, C. A., Gimeno C, et al. (2004). *Effects of a dry and warm summer conditions on CO2 and energy fluxes from three Mediterranean ecosystems*. Paper presented at the Geophys. Res. Abstr.

Savitzky, A., & Golay, M. J. (1964). Smoothing and differentiation of data by simplified least squares procedures. *Analytical chemistry, 36*(8), 1627-1639.

Schaaf, C., & Wang, Z. (2015). MCD43A4 MODIS/Terra+ Aqua BRDF/Albedo Nadir BRDF Adjusted Ref Daily L3 Global-500m V006 [Data set]. *NASA EOSDIS Land Processes DAAC*.

Schroder, I. (2014). Arcturus Emerald OzFlux tower site OzFlux: Australian and New Zealand flux research and monitoring. *hdl, 102*(100), 14249.

Scott, R. L. (2010). Using watershed water balance to evaluate the accuracy of eddy covariance evaporation measurements for three semiarid ecosystems. *Agricultural and Forest Meteorology, 150*(2), 219-225. doi:https://doi.org/10.1016/j.agrformet.2009.11.002

Scott, R. L., Biederman, J. A., Hamerlynck, E. P., & Barron-Gafford, G. A. (2015). The carbon balance pivot point of southwestern U.S. semiarid ecosystems: Insights from the 21st century drought. *Journal of Geophysical Research: Biogeosciences, 120*(12), 2612-2624. doi:https://doi.org/10.1002/2015JG003181

Scott, R. L., Jenerette, G. D., Potts, D. L., & Huxman, T. E. (2009). Effects of seasonal drought on net carbon dioxide exchange from a woody-plant-encroached semiarid grassland. *Journal of Geophysical Research: Biogeosciences, 114*(G4). doi:https://doi.org/10.1029/2008JG000900

Serrano-Ortiz, P., Domingo, F., Cazorla, A., Were, A., Cuezva, S., Villagarcía, L., Alados-Arboledas, L., & Kowalski, A. S. (2009). Interannual CO2 exchange of a sparse Mediterranean shrubland on a carbonaceous substrate. *Journal of Geophysical Research: Biogeosciences, 114*(G4). doi:https://doi.org/10.1029/2009JG000983

Shi, P., Sun, X., Xu, L., Zhang, X., He, Y., Zhang, D., & Yu, G. (2006). Net ecosystem CO2 exchange and controlling factors in a steppe—Kobresia meadow on the Tibetan Plateau. *Science in China Series D: Earth Sciences, 49*(2), 207-218. doi:10.1007/s11430-006-8207-4

Sulman, B. N., Desai, A. R., Cook, B. D., Saliendra, N., & Mackay, D. S. (2009). Contrasting carbon dioxide fluxes between a drying shrub wetland in Northern Wisconsin, USA, and nearby forests. *Biogeosciences, 6*(6), 1115-1126. doi:10.5194/bg-6-1115-2009

Suni, T., Rinne, J., Reissell, A., Altimir, N., Keronen, P., Rannik, U., Dal Maso, M., Kulmala, M., & Vesala, T. (2003). Long-term measurements of surface fluxes above a Scots pine forest in Hyytiala, southern Finland, 1996-2001. *Boreal Environment Research, 8*(4), 287-301.

Syed, K. H., Flanagan, L. B., Carlson, P. J., Glenn, A. J., & Van Gaalen, K. E. (2006). Environmental control of net ecosystem CO2 exchange in a treed, moderately rich fen in northern Alberta. *Agricultural and Forest Meteorology, 140*(1-4), 97-114.

T., M. (2016). *FLUXNET2015 US-Goo Goodwin Creek*. Retrieved from FluxNet; NOAA/ARL:

Tang, B., Zhao, X., & Zhao, W. (2018). Local effects of forests on temperatures across Europe. *Remote Sensing, 10*(4), 529.

Tang, X., Zhou, Y., Li, H., Yao, L., Ding, Z., Ma, M., & Yu, P. (2020). Remotely monitoring ecosystem respiration from various grasslands along a large-scale east–west transect across northern China. *Carbon Balance and Management, 15*, 1-14.

Tatarinov, F., Rotenberg, E., Maseyk, K., Ogée, J., Klein, T., & Yakir, D. (2016). Resilience to seasonal heat wave episodes in a Mediterranean pine forest. *New Phytologist, 210*(2), 485-496. doi:https://doi.org/10.1111/nph.13791

TEDESCHI, V., REY, A., MANCA, G., VALENTINI, R., JARVIS, P. G., & BORGHETTI, M. (2006). Soil respiration in a Mediterranean oak forest at different developmental stages after coppicing. *Global change biology, 12*(1), 110-121. doi:https://doi.org/10.1111/j.1365-2486.2005.01081.x

Thomas, C. K., Law, B. E., Irvine, J., Martin, J. G., Pettijohn, J. C., & Davis, K. J. (2009). Seasonal hydrology explains interannual and seasonal variation in carbon and water exchange in a semiarid mature ponderosa pine forest in central Oregon. *Journal of Geophysical Research: Biogeosciences, 114*(G4). doi:https://doi.org/10.1029/2009JG001010

Thum, T., Aalto, T., Laurila, T., Aurela, M., Kolari, P., & Hari, P. (2007). Parametrization of two photosynthesis models at the canopy scale in a northern boreal Scots pine forest. *Tellus Series B-Chemical and Physical Meteorology, 59*(5), 874-890. doi:10.1111/j.1600-0889.2007.00305.x

Tirone, G., Dore, S., Matteucci, G., Greco, S., & Valentini, R. (2003). Evergreen Mediterranean Forests. Carbon and Water Fluxes, Balances, Ecological and Ecophysiological Determinants. In R. Valentini (Ed.), *Fluxes of Carbon, Water and Energy of European Forests* (pp. 125-149). Berlin, Heidelberg: Springer Berlin Heidelberg.

Tramontana, G., Jung, M., Schwalm, C. R., Ichii, K., Camps-Valls, G., Ráduly, B., Reichstein, M., Arain, M. A., Cescatti, A., & Kiely, G. (2016). Predicting carbon dioxide and energy fluxes across global FLUXNET sites with regression algorithms. *Biogeosciences, 13*(14), 4291-4313.

Trautmann, T., Koirala, S., Caryalhais, N., Eicker, A., Finks, M., Niemann, C., & Jung, M. (2018). Understanding terrestrial water storage variations in northern latitudes across scales. *Hydrology and Earth System Sciences, 22*(7), 4061-4082. doi:10.5194/hess-22-4061-2018

Turner, D., Ritts, W., Styles, J., Yang, Z., Cohen, W., Law, B., & Thornton, P. (2006). A diagnostic carbon flux model to monitor the effects of disturbance and interannual variation in climate on regional NEP. *Tellus B: Chemical and Physical Meteorology, 58*(5), 476-490.

Ulke, A. G., Gattinoni, N. N., & Posse, G. (2015). Analysis and modelling of turbulent fluxes in two different ecosystems in Argentina. *International Journal of Environment and Pollution, 58*(1-2), 52-62.

Urbanski, S., Barford, C., Wofsy, S., Kucharik, C., Pyle, E., Budney, J., McKain, K., Fitzjarrald, D., Czikowsky, M., & Munger, J. W. (2007). Factors controlling CO2 exchange on timescales from hourly to decadal at Harvard Forest. *Journal of Geophysical Research: Biogeosciences, 112*(G2). doi:https://doi.org/10.1029/2006JG000293

VALENTINI, R., De ANGELIS, P., MATTEUCCI, G., MONACO, R., DORE, S., & MUCNOZZA, G. E. S. (1996). Seasonal net carbon dioxide exchange of a beech forest with the atmosphere. *Global change biology, 2*(3), 199-207. doi:https://doi.org/10.1111/j.1365-2486.1996.tb00072.x

Valentini, R., Matteucci, G., Dolman, A. J., Schulze, E. D., Rebmann, C., Moors, E. J., Granier, A., Gross, P., Jensen, N. O., Pilegaard, K., Lindroth, A., Grelle, A., Bernhofer, C., Grünwald, T., Aubinet, M., Ceulemans, R., Kowalski, A. S., Vesala, T., Rannik, Ü., Berbigier, P., et al. (2000). Respiration as the main determinant of carbon balance in European forests. *Nature, 404*(6780), 861-865. doi:10.1038/35009084

Veenendaal, E. M., Kolle, O., & Lloyd, J. (2004). Seasonal variation in energy fluxes and carbon dioxide exchange for a broad‐leaved semi‐arid savanna (Mopane woodland) in Southern Africa. *Global change biology, 10*(3), 318-328.

Vickers, D., Thomas, C., Pettijohn, C., Martin, J. G., & Law, B. (2012). Five years of carbon fluxes and inherent water-use efficiency at two semi-arid pine forests with different disturbance histories. *Tellus B: Chemical and Physical Meteorology, 64*(1), 17159. doi:10.3402/tellusb.v64i0.17159

Viovy, N. (2018). *CRUNCEP Version 7 - Atmospheric Forcing Data for the Community Land Model*. Retrieved from: https://doi.org/10.5065/PZ8F-F017

Vitale, L., Di Tommasi, P., D'Urso, G., & Magliulo, V. (2016). The response of ecosystem carbon fluxes to LAI and environmental drivers in a maize crop grown in two contrasting seasons. *International Journal of Biometeorology, 60*(3), 411-420. doi:10.1007/s00484-015-1038-2

Walther, S., Besnard, S., Nelson, J. A., El-Madany, T. S., Migliavacca, M., Weber, U., Carvalhais, N., Ermida, S. L., Bruemmer, C., Schrader, F., Prokushkin, A. S., Panov, A. V., & Jung, M. (2022). Technical note: A view from space on global flux towers by MODIS and Landsat: the FluxnetEO data set. *Biogeosciences, 19*(11), 2805-2840. doi:10.5194/bg-19-2805-2022

Wang, R., Goll, D., Balkanski, Y., Hauglustaine, D., Boucher, O., Ciais, P., Janssens, I., Penuelas, J., Guenet, B., & Sardans, J. (2017). Global forest carbon uptake due to nitrogen and phosphorus deposition from 1850 to 2100. *Global change biology, 23*(11), 4854-4872.

Weiss, A., & Norman, J. (1985). Partitioning solar radiation into direct and diffuse, visible and near-infrared components. *Agricultural and Forest Meteorology, 34*(2-3), 205-213.

Wharton, S., Falk, M., Bible, K., Schroeder, M., & Paw U, K. T. (2012). Old-growth CO2 flux measurements reveal high sensitivity to climate anomalies across seasonal, annual and decadal time scales. *Agricultural and Forest Meteorology, 161*, 1-14. doi:https://doi.org/10.1016/j.agrformet.2012.03.007

Williams, M., Law, B. E., Anthoni, P. M., & Unsworth, M. H. (2001). Use of a simulation model and ecosystem flux data to examine carbon–water interactions in ponderosa pine. *Tree Physiology, 21*(5), 287-298. doi:10.1093/treephys/21.5.287

Wohlfahrt, G., Hammerle, A., Haslwanter, A., Bahn, M., Tappeiner, U., & Cernusca, A. (2008). Seasonal and inter‐annual variability of the net ecosystem CO2 exchange of a temperate mountain grassland: Effects of weather and management. *Journal of Geophysical Research: Atmospheres, 113*(D8).

Wolf, S., Eugster, W., Ammann, C., Häni, M., Zielis, S., Hiller, R., Stieger, J., Imer, D., Merbold, L., & Buchmann, N. (2013). Contrasting response of grassland versus forest carbon and water fluxes to spring drought in Switzerland. *Environmental Research Letters, 8*(3), 035007.

Xu, T., & Hutchinson, M. (2011). ANUCLIM version 6.1 user guide. *The Australian National University, Fenner School of Environment and Society, Canberra, 90*.

Yee, M. S., Pauwels, V. R., Daly, E., Beringer, J., Rüdiger, C., McCabe, M. F., & Walker, J. P. (2015). A comparison of optical and microwave scintillometers with eddy covariance derived surface heat fluxes. *Agricultural and Forest Meteorology, 213*, 226-239.

Zhang, J.-H., Han, S.-J., & Yu, G.-R. (2006). Seasonal variation in carbon dioxide exchange over a 200-year-old Chinese broad-leaved Korean pine mixed forest. *Agricultural and Forest Meteorology, 137*(3), 150-165. doi:https://doi.org/10.1016/j.agrformet.2006.02.004

Zielis, S., Etzold, S., Zweifel, R., Eugster, W., Haeni, M., & Buchmann, N. (2014). NEP of a Swiss subalpine forest is significantly driven not only by current but also by previous year's weather. *Biogeosciences, 11*(6), 1627-1635.

Journal of Advances in Modeling Earth Systems

Supporting Information for

Towards Robust Parameterizations in Ecosystem-level Photosynthesis Models

Shanning Bao[1,2*], Lazaro Alonso[1], Siyuan Wang[1], Johannes Gensheimer[1], Ranit De[1], Nuno Carvalhais[1,3,4*]

[1]Department for Biogeochemical Integration, Max-Planck-Institute for Biogeochemistry, 07745, Jena, Germany.

[2]National Space Science Center, Chinese Academy of Sciences, 100190, Beijing, China.

[3]Departamento de Ciências e Engenharia do Ambiente, DCEA, Faculdade de Ciências e Tecnologia, FCT, Universidade Nova de Lisboa, 2829-516 Caparica, Portugal.

[4]ELLIS Unit Jena, 07745, Jena, Germany.

Contents of this file

Introduction

The supporting information includes the descriptions of model parameters calibration (text S1), cost functions used in SPIE (text S2), and figures and tables to supplement the information about the data and results appeared in the main text.

Text S1. Model parameters calibration

To get the highest model performance, we here calibrated the LUE model at each site using the full time series of GPP_{obs}. The purpose of model calibration is to find the parameter vector that can minimize the cost function, a metric to measure the model error, and to reduce

the model uncertainties associated with model parameters. In the calibration process, the parameters were optimized in their physical ranges (Table 1) using a stochastic and derivative-free evolutionary algorithm, CMAES(Hansen & Kern, 2004). CMAES, which is a reliable tool for global optimization (Trautmann et al., 2018).

We define the cost function (*cf*) as the sum of the GPP errors (cf_1, equation S- 2), the ET errors (cf_2, equation S- 3), and the environmental sensitivity functions (*f*X) constraints (cf_3 and cf_4).

$$cf = cf_1 + cf_2 + (cf_3 + cf_4) \qquad \text{S- 1}$$

$$cf_1 = \sum_{t=1}^{N_t} \sqrt{\left(GPP_t - \widehat{GPP}_t\right)^2 \cdot \sigma_{NEE_t}^{-2}} \qquad \text{S- 2}$$

$$cf_2 = \sum_{t=1}^{N_t} \sqrt{\left(ET_t - \widehat{ET}_t\right)^2 \cdot \sigma_{LE_t}^{-2}} \qquad \text{S- 3}$$

The cf_1 and cf_2 are to measure the sum of squares for errors of simulated GPP and ET, which is used to optimize the parameters of water availability index (WAI, see Table S2), at each time step *t*. The simulated GPP using the calibrated LUE parameters ($\widehat{GPP}$) and simulated ET using the calibrated WAI parameters ($\widehat{ET}$) were compared to GPP_{obs} (*GPP*) and ET_{obs} (*ET*), respectively. N_t denotes the total number of time steps. Due to the uncertainties in observation and the different units of GPP and ET, we weighted the model errors using the estimated uncertainty of *GPP* (σ_{NEE}) and *ET* (σ_{LE}), respectively. We assume that the parameter vector that minimizes the sum of cf_1 and cf_2 is the best for the LUE model and WAI, respectively.

We follow the concept of ecological and dynamic constraints (EDC, by (Bloom & Williams, 2015)) to regularize the inversion approach via two additional constraints: cf_3 (equation S- 4) and cf_4 (equation S- 5).

$$cf_3 = \left(\left(1\text{-}\max(f\mathrm{T}_r)\right) + \left(1\text{-}\max(f\mathrm{VPD}_r)\right) + \left(1\text{-}\max(f\mathrm{W}_r)\right) + \left(1\text{-}\max(f\mathrm{L}_r)\right)\right) \cdot c \qquad \text{S- 4}$$

$$cf_4 = \left(\sum_r\left(fT_r(T<0\,°C) > \theta_{fT}\right) + \sum_r\left(fVPD_r(VPD>2kPa) > \theta_{fVPD}\right) + \sum_r\left(fW_r(W<0.01) > \theta_{fW}\right)\right) \cdot c \qquad \text{S- 5}$$

These impose constraints on the simulated *f*X (i.e., *f*T, *f*VPD, *f*W, *f*L and *f*CI) based on two assumptions: the instantaneous ε ($=\varepsilon_{max} \cdot fT \cdot fVPD \cdot fW \cdot fL \cdot fCI$) of vegetation can reach its potential, ε_{max}, under some specific environmental condition (cf_3) and is inhibited under a non-ideal growing condition (cf_4). Here cf_3 and cf_4 were calculated independently from cf_1 and cf_2, using analog inputs (PAR=0-20 $MJ \cdot m^{-2} \cdot day^{-1}$, FAPAR=0-1, T=-10-40 °C, VPD=0-2 kPa, W=0-1 and CI=0-1). *cf*3 is to set the maximum of *f*T, *f*VPD, excluding the CO_2 fertilization effect (the right part of equation 3), *f*W, and *f*L to one, which implies that the corresponding environmental factor does not limit ε at a certain point within the given ranges of PAR$\in$ [0,20] (in $MJ \cdot m^{-2} \cdot day^{-1}$), FAPAR$\in$[0,1], T$\in$[-10,40] (in °C), VPD$\in$[0,2] (in kPa), W$\in$[0,1] and CI$\in$[0,1], represented by the subscript, *r*, in equations S- 4-S- 5 (e.g., $\max(fT_r)$ represents the maximum *f*T when the temperature is ranging between -10 and 40 °C).

Another constraint, cf_4, is to guarantee the *f*T, *f*VPD, excluding the CO_2 fertilization part, and *f*W lower than the threshold (θ_{fT}, θ_{fVPD}, and θ_{fW}) under the non-ideal conditions (T<0 °C, VPD>2 kPa, or W<0.01). Here the thresholds (θ_{fT}=0.2, θ_{fVPD}=0.9, and θ_{fW}=0.2) were estimated according to the normalized ratio of GPP to APAR at all sites. The other non-ideal conditions were not included since they vary across sites. The *c* in equations S- 4-S- 5 denotes a penalty term ($=10^4$, an empirical value) to coordinate the scales of cf_1, cf_2, cf_3, and cf_4.

Since the WAI parameters were not predicted in this study, the calibrated WAI parameters were used in the parameterization experiments and the cf_2 was not considered in the optimization-based parameterization methods, i.e., 'OPT-All' and 'OPT-PFT'.

Text S2. Cost functions used in SPIE

The cost function (cf_{NN}, equation S- 6) for SPIE was similar to the sum of cf_1, cf_3, and cf_4. Since normalizing the cost function can significantly improve the training efficiency of neural network, we used normalized NSE (Nossent & Bauwens, 2012), ranging from 0-1, rather than the sum of squares (S- 7).

$$cf_{\mathrm{NN}}=cf_{\mathrm{NN1}}+cf_3+cf_4 \qquad S\text{-}6$$

$$cf_{\mathrm{NN1}}=\frac{\sum_{t=1}^{N_t}\left(GPP_t-\widehat{GPP}_t\right)^2\cdot\sigma_{NEE_t}^{-2}}{\sum_{t=1}^{N_t}\left(GPP_t-\widehat{GPP}_t\right)^2\cdot\sigma_{NEE_t}^{-2}+\sum_{t=1}^{N_t}\left(GPP_t-\overline{GPP}\right)^2\cdot\sigma_{NEE_t}^{-2}} \qquad S\text{-}7$$

GPP_t and $\widehat{GPP}_t$ are the observed and simulated GPP at time step, t. The normalized NSE is the ratio between the sum of the GPP errors across all time steps (N_t) to the sum of GPP errors and the sum of GPP changes to the average GPP ($\overline{GPP}$). To consider the EDC, we added cf_{NN1} to cf_3 and cf_4 as defined in section S1. The only difference was that the empirical coefficient, c, was changed to 0.2 here due to the small range of cf_{NN1}.

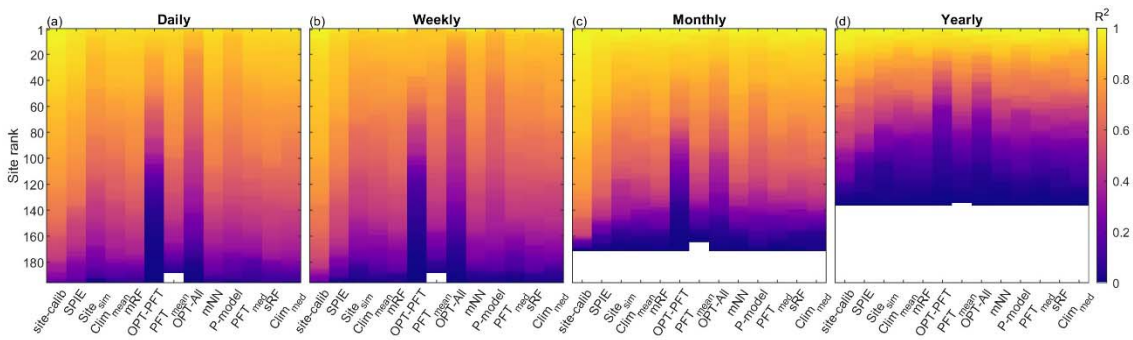

Figure S1. Comparison of R^2 between GPP_{obs} and GPP_{sim} based on twelve different parameterization methods, and between GPP_{obs} and GPP_{calib} (site-calib) at daily (a), weekly (b), monthly (c) and yearly (d) scales. The sites with less than four good-quality months or years are removed from panel c and d, respectively. The sites with p-value larger than 0.05 are shown in white**.**

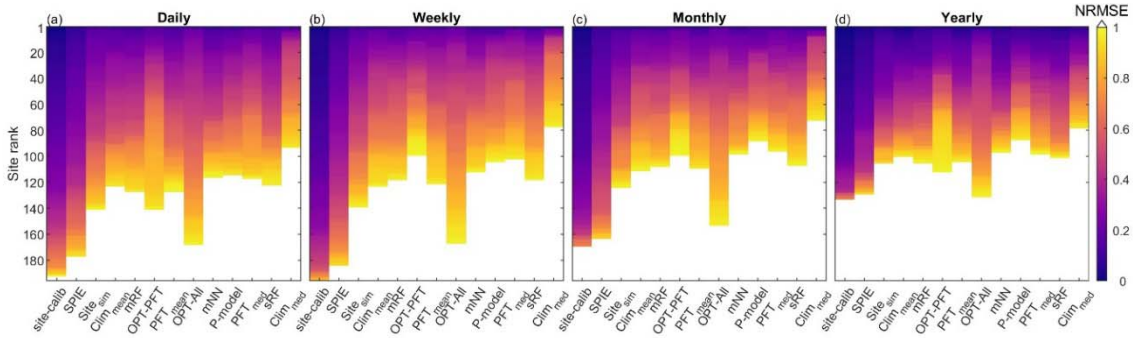

Figure S2. Comparison of NRMSE between GPP_{obs} and GPP_{sim} based on twelve different parameterization methods, and between GPP_{obs} and GPP_{calib} (site-calib) at daily (a), weekly (b), monthly (c) and yearly (d) scales.

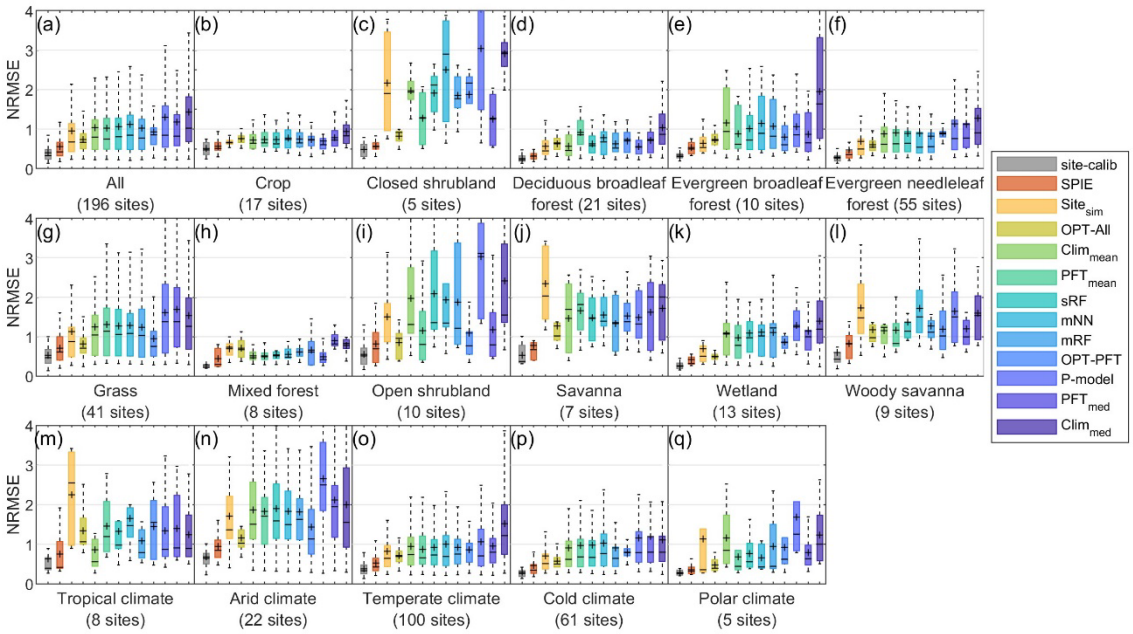

Figure S3. Site-level daily NRMSE comparison across all sites (a), per PFT (b-l) and per Clim (m-q). The mean and median per type are represented by the black cross and line, respectively

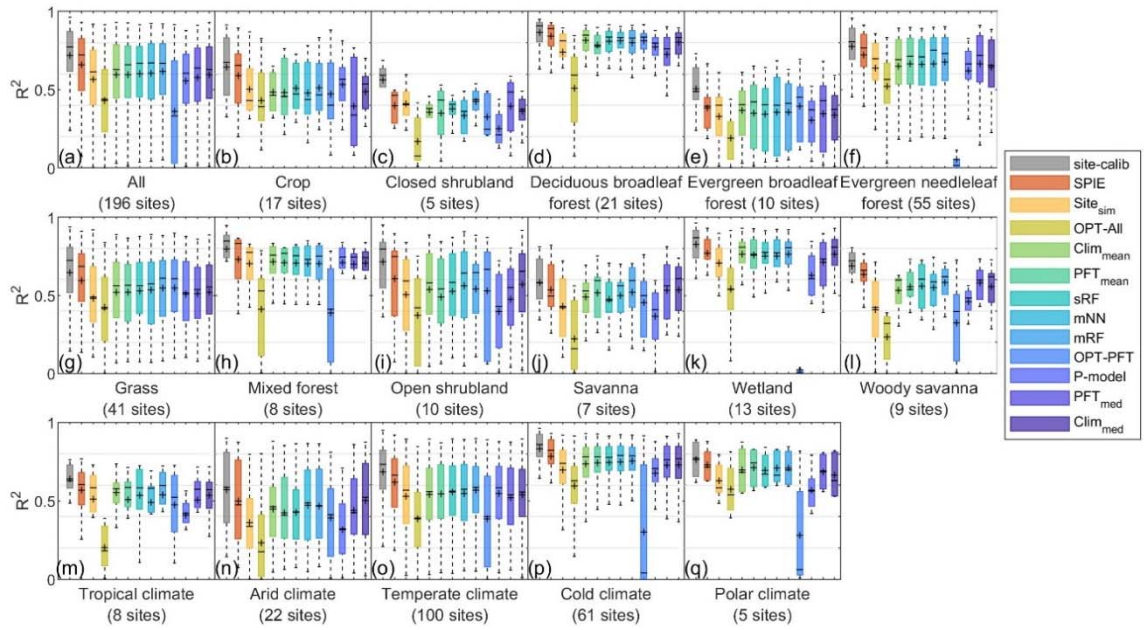

Figure S4. Site-level daily R^2 comparison across all sites (a), per PFT (b-l) and per Clim (m-q). The mean and median per type are represented by the black cross and line, respectively

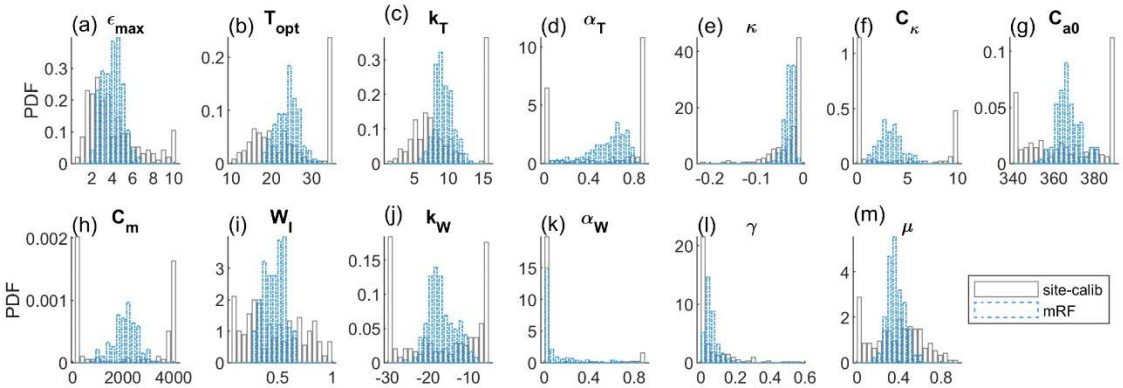

Figure S5. The probability distribution function (PDF) of the predicted parameters by mRF (Upscal) and the calibrated parameters (Calib)

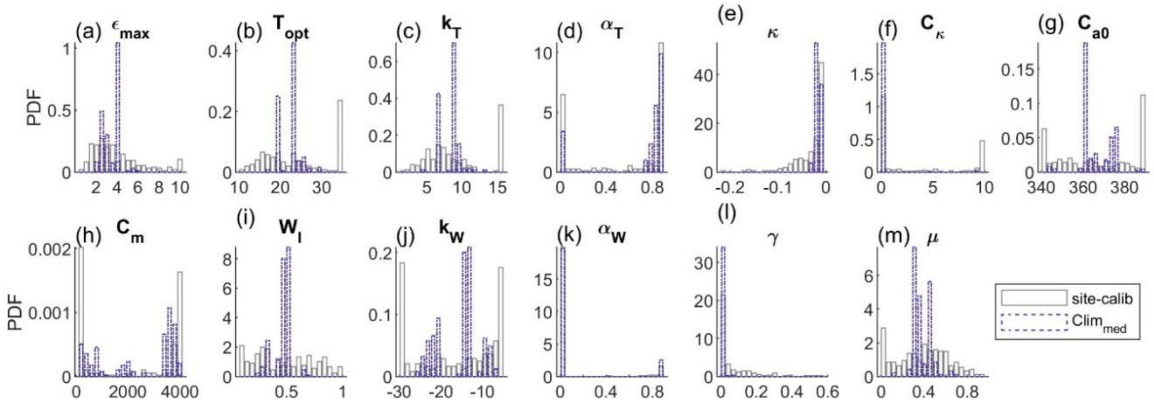

Figure S6. The probability distribution function (PDF) of the predicted parameters by $Clim_{med}$ and the calibrated parameters

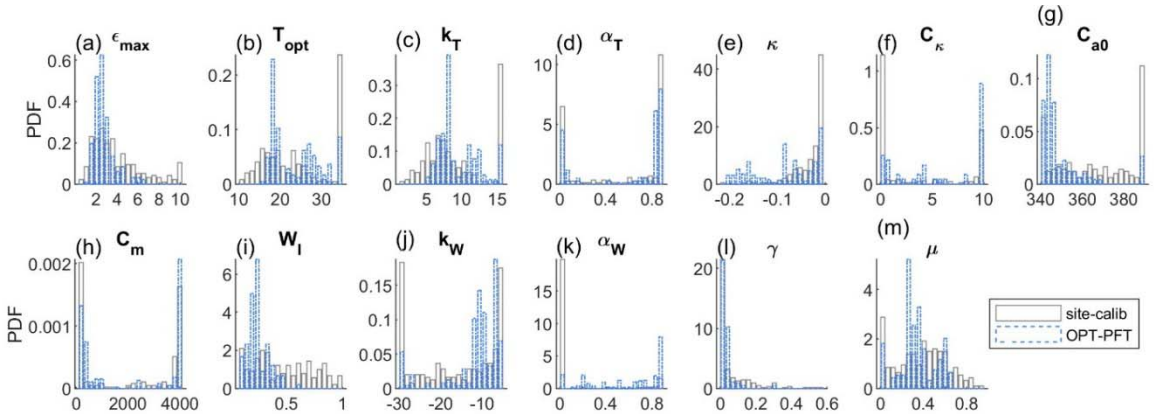

Figure S7. The probability distribution function (PDF) of the predicted parameters by OPT-PFT and the calibrated parameters

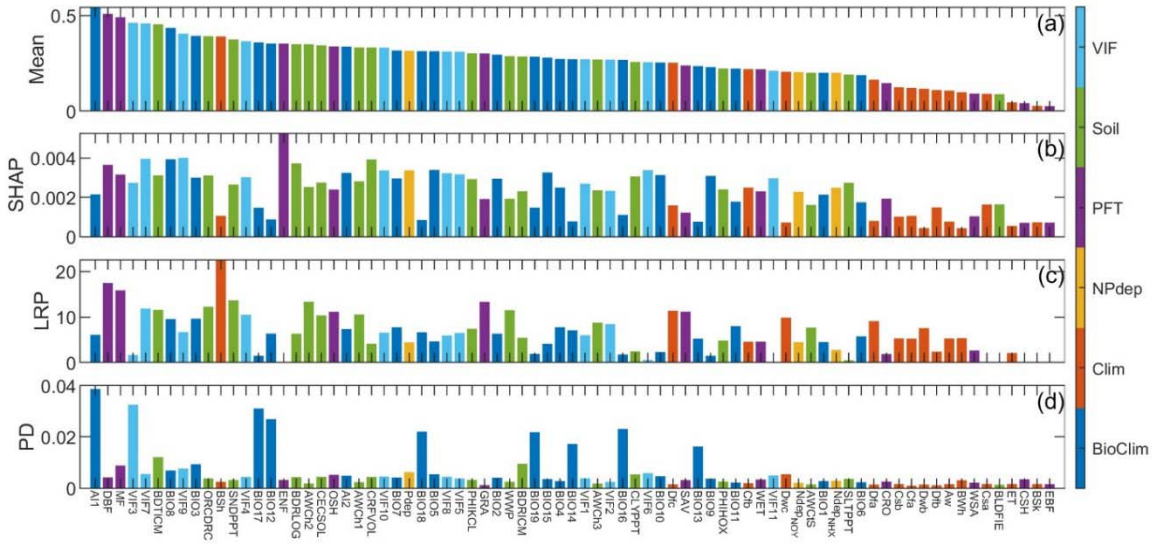

Figure S8. The input features for predicting LUE model parameters sorted according to the average normalized SHAP, LRP and PD values (a). The absolute SHAP, LRP and PD of each feature are shown in b-d in the same order.

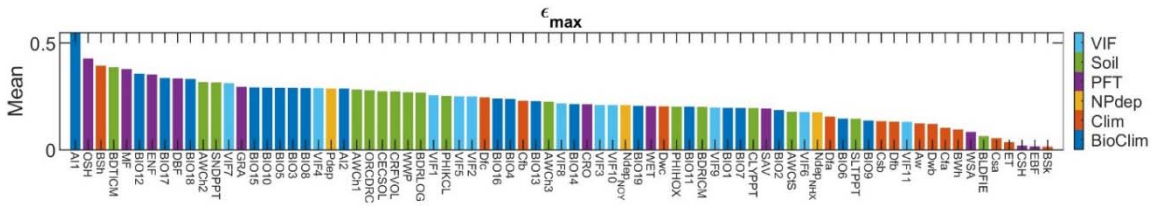

Figure S9. The features sorted by the average normalized SHAP, LRP and PD for ε_{max}

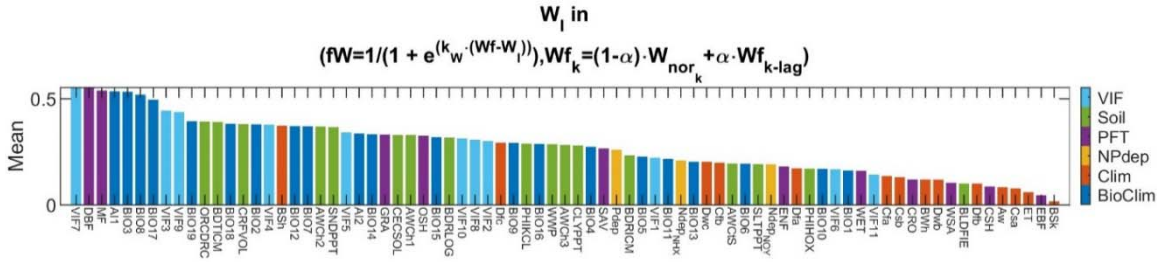

Figure S10. The features sorted by the average normalized SHAP, LRP and PD for W_l

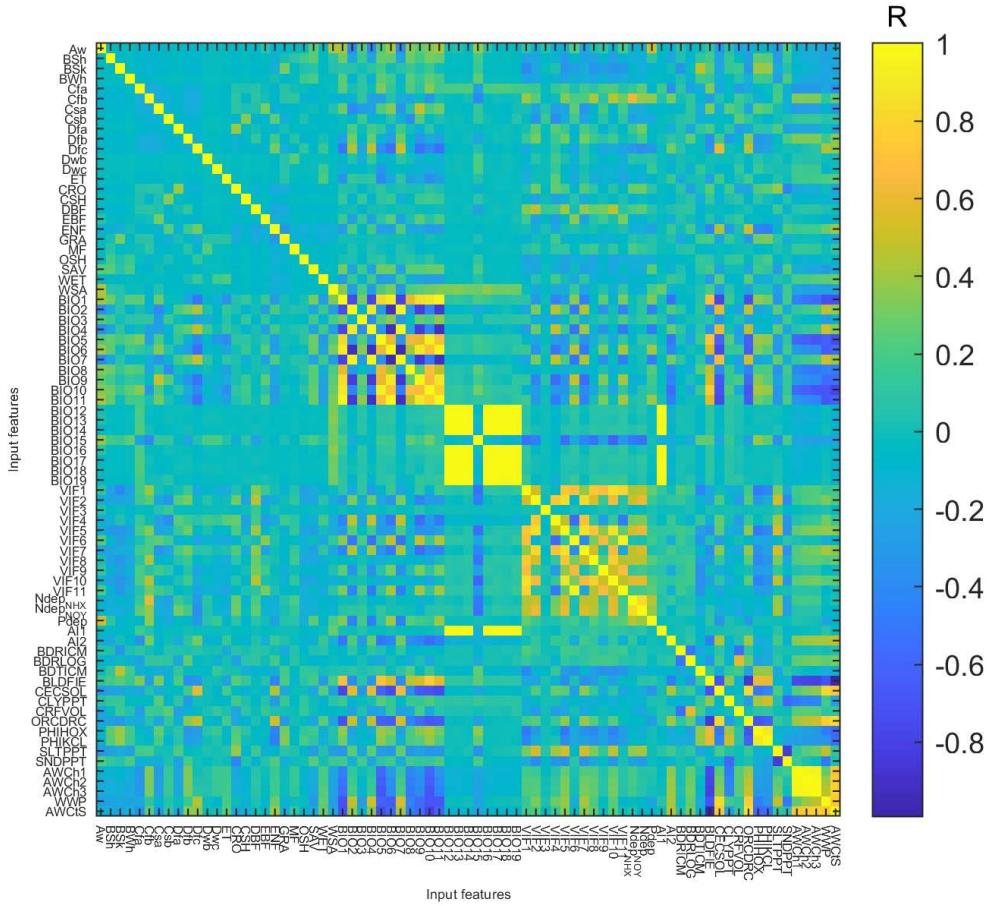

Figure S11. Correlation coefficient (R) matrix between input features.

Table S1. Eddy covariance flux site list used in this study. The latitude (Lat), longitude (Lon) and plant functional types (PFT) are collected from FLUXNET website. The data length differs across site and is determined by the years between 'data start' and 'data end'. The climate type is extracted from the Koeppen-Geiger climate classification map (at 5 arc min; Rubel et al., 2017). The elevation is collected from the site ancillary information, papers and satellite images (see the footnote below the table). The site group refers to the group number of each site used to validate the training result.

SiteID	Lat	Lon	Data start (year)	Data end (year)	PFT	Climate type	Elevation (m)	Site group	Reference
AR-SLu	-33.5	-66.5	2010	2011	MF	BSh	506*e	4	(Ulke et al., 2015)
AT-Neu	47.1	11.3	2002	2012	GRA	Dfc	970	10	(Wohlfahrt et al., 2008)
AU-ASM	-22.3	133.3	2010	2014	ENF	BWh	606*b	5	(Cleverly et al., 2013)

AU-Cpr	-34.0	140.6	2010	2014	SAV	BSk	62[*e]	3	(Bloomfield et al., 2018; Meyer et al., 2015)
AU-Cum	-33.6	150.7	2012	2014	EBF	Cfa	20	1	(Renchon et al., 2018)
AU-DaP	-14.1	131.3	2009	2013	GRA	Aw	71[*e]	3	(Hutley et al., 2011)
AU-DaS	-14.2	131.4	2010	2014	SAV	Aw	110	6	(Hutley et al., 2011)
AU-Dry	-15.3	132.4	2008	2014	SAV	Aw	175	5	(Hutley et al., 2011)
AU-Emr	-23.9	148.5	2011	2013	GRA	BSh	170	3	(Schroder, 2014)
AU-Gin	-31.4	115.7	2013	2014	WSA	Csa	51	3	(Beringer et al., 2016)
AU-GWW	-30.2	120.7	2011	2014	SAV	BSh	450	1	(Beringer et al., 2016)
AU-How	-12.5	131.2	2001	2014	WSA	Aw	64	2	(Beringer et al., 2003)
AU-RDF	-14.6	132.5	2011	2013	WSA	Aw	188[*e]	7	(Bristow et al., 2016)
AU-Rig	-36.7	145.6	2011	2014	GRA	Cfa	152	10	(Beringer et al., 2016)
AU-Stp	-17.2	133.4	2008	2014	GRA	BSh	250[*b]	1	(Hutley et al., 2011)
AU-TTE	-22.3	133.6	2012	2014	OSH	BWh	553	3	(Cleverly et al., 2016)
AU-Tum	-35.7	148.2	2001	2014	EBF	Cfb	1200	8	(Leuning et al., 2005)
AU-Wom	-37.4	144.1	2010	2014	EBF	Cfb	705	6	(Griebel et al., 2016)
AU-Ync	-35.0	146.3	2012	2014	GRA	BSk	126[*e]	6	(Yee et al., 2015)
BE-Bra	51.3	4.5	2000	2014	MF	Cfb	16[*a]	7	(Carrara et al., 2004)
BE-Lon	50.6	4.8	2004	2014	CRO	Cfb	167	2	(Aubinet et al., 2009)
BE-Vie	50.3	6.0	2000	2014	MF	Cfb	450[*a]	1	As above
BR-Ban	-9.8	-50.2	2003	2006	EBF	Aw	120	6	(Da Rocha et al., 2009)
BR-Sp1	-21.6	-47.7	2001	2002	WSA	Aw	690	9	As above
BW-Ma1	-19.9	23.6	2000	2001	WSA	BSh	950	4	(Veenendaal et al., 2004)

CA-Ca1	49.9	-125.3	2000	2005	ENF	Cfb	300	7	(Humphreys et al., 2006)
CA-Ca2	49.9	-125.3	2000	2005	ENF	Csb	300	7	As above
CA-Ca3	49.5	-124.9	2001	2005	ENF	Csb	300	7	As above
CA-Gro	48.2	-82.2	2003	2014	MF	Dfb	340	9	(Pejam et al., 2006)
CA-Let	49.7	-112.9	2000	2005	GRA	BSk	960	7	(Flanagan et al., 2002)
CA-Mer	45.4	-75.5	2000	2005	WET	Dfb	70	1	(Lafleur et al., 2003)
CA-NS2	55.9	-98.5	2002	2005	ENF	Dfc	260	6	(Beringer et al., 2011)
CA-NS3	55.9	-98.4	2001	2005	ENF	Dfc	260	10	As above
CA-NS4	55.9	-98.4	2002	2005	ENF	Dfc	260	6	As above
CA-NS5	55.9	-98.5	2002	2005	ENF	Dfc	260	2	As above
CA-NS6	55.9	-99.0	2001	2005	OSH	Dfc	244	2	As above
CA-NS7	56.6	-100.0	2002	2005	OSH	Dfc	297	5	As above
CA-Oas	53.6	-106.2	2000	2010	DBF	Dfc	530	6	(Black et al., 1996)
CA-Obs	54.0	-105.1	2000	2010	ENF	Dfc	628.94	7	(Jarvis et al., 1997)
CA-Ojp	53.9	-104.7	2000	2005	ENF	Dfb	579	1	(Baldocchi et al., 1997)
CA-Qcu	49.3	-74.0	2001	2006	ENF	Dfb	392.3	4	(Giasson et al., 2006)
CA-Qfo	49.7	-74.3	2004	2010	ENF	Dfc	382	7	(Bergeron et al., 2007)
CA-SF1	54.5	-105.8	2003	2006	ENF	Dfc	536	10	(Mkhabela et al., 2009)
CA-SF2	54.3	-105.9	2001	2005	ENF	Dfc	520	6	As above
CA-SF3	54.1	-106.0	2001	2005	OSH	Dfc	540	5	As above
CA-SJ1	53.9	-104.7	2001	2005	ENF	Dfb	580	8	(Howard et al., 2004)
CA-SJ2	53.9	-104.7	2003	2005	ENF	Dfc	580	1	(Coursolle et al., 2012)
CA-TP1	42.7	-80.6	2008	2014	ENF	Dfb	265	4	(Peichl & Arain, 2007)
CA-TP3	42.7	-80.4	2008	2014	ENF	Dfb	184	2	As above

CA-TP4	42.7	-80.4	2008	2014	ENF	Dfb	184	8	(Arain & Restrepo-Coupe, 2005)
CA-TPD	42.6	-80.6	2012	2014	DBF	Dfb	260	1	As above
CA-WP1	55.0	-112.5	2003	2005	WET	Dfc	540	4	(Syed et al., 2006)
CH-Cha	47.2	8.4	2005	2014	GRA	Cfb	393	5	(Lutz Merbold et al., 2014)
CH-Dav	46.8	9.9	2000	2014	ENF	ET	1639	9	(Wolf et al., 2013; Zielis et al., 2014)
CH-Fru	47.1	8.5	2005	2014	GRA	Cfb	982	3	(Imer et al., 2013)
CH-Oe1	47.3	7.7	2002	2008	GRA	Cfb	450	3	(Ammann et al., 2009)
CN-Cha	42.4	128.1	2003	2005	MF	Dwb	738	1	(Zhang et al., 2006)
CN-Cng	44.6	123.5	2007	2010	GRA	BSk	171[*d]	10	(Pastorello et al., 2020)
CN-Dan	30.5	91.1	2004	2005	GRA	Dwc	4286	8	(Shi et al., 2006)
CN-Du2	42.1	116.3	2006	2008	GRA	Dwb	1350[*b]	5	(Chen et al., 2009)
CN-Ha2	37.6	101.3	2003	2005	WET	Dwc	3357	2	(Pastorello et al., 2020)
CN-Xfs	44.1	116.3	2004	2006	GRA	BSk	1250	4	(Chen et al., 2009)
CZ-BK1	49.5	18.5	2004	2014	ENF	Dfb	908[*a]	8	(Krupková et al., 2017)
CZ-BK2	49.5	18.5	2009	2012	GRA	Dfb	855	7	(Acosta et al., 2013)
CZ-wet	49.0	14.8	2007	2014	WET	Cfb	426	3	(Dušek et al., 2012)
DE-Geb	51.1	10.9	2001	2014	CRO	Cfb	161.5	7	(Anthoni et al., 2004b)
DE-Gri	51.0	13.5	2004	2014	GRA	Cfb	385	4	(Prescher et al., 2010)
DE-Hai	51.1	10.5	2000	2009	DBF	Cfb	430[*a]	9	(Knohl et al., 2003)
DE-Har	47.9	7.6	2005	2006	ENF	Cfb	201	1	(Pastorello et al., 2020)

DE-Kli	50.9	13.5	2004	2014	CRO	Cfb	478	8	(Prescher et al., 2010)
DE-Lnf	51.3	10.4	2002	2012	DBF	Cfb	451	9	(Anthoni et al., 2004a)
DE-Meh	51.3	10.7	2003	2006	MF	Cfb	293[*a]	7	(DON et al., 2009)
DE-Obe	50.8	13.7	2008	2014	ENF	Cfb	734	4	(Pastorello et al., 2020)
DE-SfN	47.8	11.3	2013	2014	WET	Cfb	590	2	(Hommeltenberg et al., 2014)
DE-Tha	51.0	13.6	2000	2014	ENF	Cfb	380[*a]	3	(Bernhofer et al., 2003)
DE-Wet	50.5	11.5	2002	2006	ENF	Cfb	785[*a]	8	(Rebmann et al., 2010)
DK-Ris	55.5	12.1	2004	2005	CRO	Cfb	10	10	(Pastorello et al., 2020)
DK-Sor	55.5	11.6	2000	2014	DBF	Cfb	40[*a]	10	(Pilegaard & Ibrom, 2020)
ES-Amo	36.8	-2.3	2000	2014	OSH	BSh	58	3	(López-Ballesteros et al., 2017)
ES-ES1	39.4	-0.3	2007	2012	ENF	Csa	5[*a]	3	(Sanz M J, 2004)
ES-ES2	39.3	-0.3	2000	2006	CRO	Csa	10	9	As above
ES-LgS	37.1	-3.0	2004	2006	OSH	Csb	2267	9	(Reverter et al., 2010)
ES-LJu	36.9	-2.8	2005	2011	OSH	Csa	1600	6	(Serrano-Ortiz et al., 2009)
ES-LMa	39.9	-5.8	2004	2006	SAV	Csa	258[*a]	5	(Perez-Priego et al., 2017)
ES-VDA	42.2	1.5	2007	2009	GRA	Cfb	1765[*a]	2	(Pastorello et al., 2020)
FI-Hyy	61.9	24.3	2004	2006	ENF	Dfc	181[*a]	8	(Suni et al., 2003)
FI-Kaa	69.1	27.3	2000	2014	WET	Dfc	155	2	(MIKA AURELA et al., 2007)
FI-Let	60.6	24.0	2000	2006	ENF	Dfb	111	5	(Koskinen et al., 2014)
FI-Lom	68.0	24.2	2009	2012	WET	Dfc	269[*a]	2	(M. Aurela et al., 2015)

FI-Sod	67.4	26.6	2007	2009	ENF	Dfc	180[*a]	1	(Thum et al., 2007)
FR-Fon	48.5	2.8	2008	2014	DBF	Cfb	92[*a]	8	(Michelot et al., 2011)
FR-Gri	48.8	2.0	2005	2013	CRO	Cfb	125	6	(Loubet et al., 2011)
FR-Hes	48.7	7.1	2004	2014	DBF	Cfb	300[*a]	2	(Granier et al., 2000)
FR-LBr	44.7	-0.8	2000	2006	ENF	Cfb	61[*a]	1	(Berbigier et al., 2001)
FR-Lq1	45.6	2.7	2000	2008	GRA	Cfb	1040	9	(Pastorello et al., 2020)
FR-Lq2	45.6	2.7	2004	2006	GRA	Cfb	1040	1	(Pastorello et al., 2020)
FR-Pue	43.7	3.6	2004	2006	EBF	Csa	270[*a]	5	(Rambal et al., 2004)
GL-ZaH	74.5	-20.6	2000	2014	GRA	ET	48	4	(Lund et al., 2012)
HU-Bug	46.7	19.6	2002	2006	GRA	Cfb	111[*a]	7	(Pastorello et al., 2020)
IL-Yat	31.3	35.1	2001	2006	ENF	Csa	650	7	(Tatarinov et al., 2016)
IT-Amp	41.9	13.6	2002	2006	GRA	Cfb	884[*a]	6	(Papale et al., 2015)
IT-BCi	40.5	15.0	2004	2012	CRO	Csa	20	7	(Vitale et al., 2016)
IT-CA1	42.4	12.0	2011	2014	DBF	Csa	200	4	(Sabbatini et al., 2016)
IT-CA2	42.4	12.0	2011	2014	CRO	Csa	200	5	(Sabbatini et al., 2016)
IT-CA3	42.4	12.0	2011	2014	DBF	Csa	197	5	(Sabbatini et al., 2016)
IT-Col	41.9	13.6	2004	2014	DBF	Cfb	1560[*a]	4	(VALENTINI et al., 1996)
IT-Cpz	41.7	12.4	2000	2008	EBF	Csa	68	8	(Tirone et al., 2003)
IT-Isp	45.8	8.6	2013	2014	DBF	Cfa	210	9	(Ferréa et al., 2012)
IT-Lav	46.0	11.3	2004	2014	ENF	Cfb	1353	2	(B. Marcolla et al., 2003)
IT-Lec	43.3	11.3	2005	2006	EBF	Csa	314	8	(Pastorello et al., 2020)

IT-MBo	46.0	11.1	2003	2013	GRA	Dfb	1550[*a]	5	(Barbara Marcolla et al., 2005)
IT-Noe	40.6	8.2	2004	2014	CSH	Csa	25	10	(Papale et al., 2015)
IT-Non	44.7	11.1	2001	2006	MF	Cfa	25[*c]	1	(Nardino, 2002)
IT-PT1	45.2	9.1	2002	2004	DBF	Cfa	60	8	(Migliavacca et al., 2009)
IT-Ren	46.6	11.4	2002	2013	ENF	Dfc	1730[*a]	10	(Barbara Marcolla et al., 2005)
IT-Ro1	42.4	11.9	2000	2008	DBF	Csa	235	9	(Rey et al., 2002)
IT-Ro2	42.4	11.9	2002	2012	DBF	Csa	224[*a]	4	(TEDESCHI et al., 2006)
IT-SR2	43.7	10.3	2013	2014	ENF	Csa	4	10	(Pastorello et al., 2020)
IT-SRo	43.7	10.3	2000	2012	ENF	Csa	4[*a]	7	(Chiesi et al., 2005)
IT-Tor	45.8	7.6	2008	2012	GRA	ET	2160	10	(Galvagno et al., 2013)
NL-Ca1	52.0	4.9	2003	2006	GRA	Cfb	0.7	3	(Jacobs et al., 2007)
NL-Loo	52.2	5.7	2000	2014	ENF	Cfb	25[*a]	9	(Dolman et al., 2002)
PT-Cor	39.1	-8.3	2010	2017	EBF	Csa	170[*c]	6	(Pastorello et al., 2020)
PT-Esp	38.6	-8.6	2002	2006	EBF	Csa	95[*a]	9	(Rodrigues et al., 2011)
PT-Mi1	38.5	-8.0	2003	2005	EBF	Csa	264[*a]	10	(Pereira et al., 2007)
PT-Mi2	38.5	-8.0	2004	2006	GRA	Csa	190	8	(Pereira et al., 2007)
RU-Fyo	56.5	32.9	2002	2014	ENF	Dfb	265[*a]	9	(Kurbatova et al., 2008)
RU-Ha1	54.7	90.0	2002	2004	GRA	Dfb	446	4	(Belelli Marchesini et al., 2007)
RU-Zot	60.8	89.4	2002	2004	ENF	Dfc	90	10	(Arneth et al., 2002)
SD-Dem	13.3	30.5	2007	2009	SAV	BWh	500	2	(Ardö et al., 2008)

SE-Deg	64.2	19.6	2001	2005	WET	Dfc	270	6	(Sagerfors et al., 2008)
SE-Fla	64.1	19.5	2000	2002	ENF	Dfc	226*c	3	(Valentini et al., 2000)
US-AR1	36.4	-99.4	2009	2012	GRA	Cfa	611	6	(Billesbach D, 2016)
US-AR2	36.6	-99.6	2009	2012	GRA	Cfa	646	10	(Billesbach D, 2016)
US-ARb	35.6	-98.0	2003	2012	GRA	Cfa	424	8	(Pastorello et al., 2020)
US-ARc	35.6	-98.0	2005	2006	GRA	Cfa	424	5	(Pastorello et al., 2020)
US-ARM	36.6	-97.5	2005	2006	CRO	Cfa	314	2	(Pastorello et al., 2020)
US-Atq	70.5	-157.4	2003	2008	WET	ET	15	10	(Pastorello et al., 2020)
US-Aud	31.6	-110.5	2002	2006	GRA	BSk	1469	9	(Pastorello et al., 2020)
US-Bar	44.1	-71.3	2004	2005	DBF	Dfb	272	8	(Ouimette et al., 2018)
US-Bkg	44.4	-96.8	2004	2006	GRA	Dfa	510	4	(Gilmanov et al., 2005)
US-Blo	38.9	-120.6	2000	2007	ENF	Csb	1315	1	(Goldstein et al., 2000)
US-Bo1	40.0	-88.3	2000	2007	CRO	Cfa	219	2	(Pastorello et al., 2020)
US-Bo2	40.0	-88.3	2004	2006	CRO	Cfa	219	9	(Pastorello et al., 2020)
US-Cop	38.1	-109.4	2011	2013	GRA	BSk	1520	1	(D., 2016)
US-CRT	41.6	-83.4	2001	2007	CRO	Dfa	180	8	(Pastorello et al., 2020)
US-Dk1	36.0	-79.1	2001	2005	GRA	Cfa	168	7	(Pastorello et al., 2020)
US-Dk3	36.0	-79.1	2001	2005	ENF	Cfa	163	4	(Pastorello et al., 2020)

US-Fmf	35.1	-111.7	2000	2006	ENF	Csb	2160	5	(Pastorello et al., 2020)
US-FPe	48.3	-105.1	2004	2006	GRA	BSk	634	3	(Pastorello et al., 2020)
US-FR2	30.0	-98.0	2005	2006	WSA	Cfa	271.9	5	(Heinsch et al., 2004)
US-Goo	34.3	-89.9	2002	2006	GRA	Cfa	87	10	(T., 2016)
US-Ha1	42.5	-72.2	2000	2012	DBF	Dfb	340	2	(Urbanski et al., 2007)
US-Ho1	45.2	-68.7	2000	2004	ENF	Dfb	60	10	(Hollinger et al., 1999)
US-IB1	41.9	-88.2	2005	2007	CRO	Dfa	226.5	3	(Pastorello et al., 2020)
US-IB2	41.8	-88.2	2004	2011	GRA	Dfa	226.5	5	(Pastorello et al., 2020)
US-Ivo	68.5	-155.8	2004	2007	WET	ET	568	1	(Epstein et al., 2004)
US-KS2	28.6	-80.7	2003	2006	CSH	Cfa	3	6	(Powell et al., 2006)
US-Los	46.1	-90.0	2000	2014	WET	Dfb	480	4	(Sulman et al., 2009)
US-Me2	44.5	-121.6	2000	2014	ENF	Csb	1253	2	(Kwon et al., 2018; Thomas et al., 2009)
US-Me3	44.3	-121.6	2004	2006	ENF	Csb	1005	6	(Vickers et al., 2012)
US-Me5	44.4	-121.6	2002	2014	ENF	Csb	1188	4	(Law et al., 2001; Williams et al., 2001)
US-Me6	44.3	-121.6	2004	2009	ENF	Csb	998	7	(Ruehr et al., 2014)
US-MMS	39.3	-86.4	2000	2002	DBF	Cfa	275	7	(Roman et al., 2015)
US-MOz	38.7	-92.2	2010	2014	DBF	Cfa	219.4	3	(Gu et al., 2016)
US-Myb	38.1	-121.8	2011	2014	WET	Csa	-1	2	(Pastorello et al., 2020)
US-NC1	35.8	-76.7	2005	2006	OSH	Cfa	5	4	(Noormets et al., 2012)

US-NC2	35.8	-76.7	2005	2006	ENF	Cfa	5	2	(Pastorello et al., 2020)
US-Ne1	41.2	-96.5	2000	2014	CRO	Dfa	361	7	(Pastorello et al., 2020)
US-Ne2	41.2	-96.5	2001	2013	CRO	Dfa	362	8	(Pastorello et al., 2020)
US-Ne3	41.2	-96.4	2001	2013	CRO	Dfa	363	6	(Pastorello et al., 2020)
US-NR1	40.0	-105.6	2001	2013	ENF	Dfc	3050	9	(Monson et al., 2002)
US-Oho	41.6	-83.8	2004	2013	DBF	Dfa	230	4	(DeForest et al., 2006)
US-Prr	65.1	-147.5	2011	2014	ENF	Dfc	210	3	(Ikawa et al., 2015; Nakai et al., 2013)
US-SO2	33.4	-116.6	2004	2006	CSH	Csb	1394	3	(Lipson et al., 2005)
US-SO3	33.4	-116.6	2001	2006	CSH	Csb	1429	5	(Lipson et al., 2005)
US-SO4	33.4	-116.6	2004	2006	CSH	Csb	1429	5	(Lipson et al., 2005)
US-SP2	29.8	-82.2	2000	2004	ENF	Cfa	50	9	(Clark et al., 1999)
US-SP3	29.8	-82.2	2000	2004	ENF	Cfa	50	6	(Clark et al., 1999)
US-SRC	31.9	-110.8	2008	2014	OSH	BSh	991	6	(Pastorello et al., 2020)
US-SRG	31.8	-110.8	2008	2014	GRA	Csa	1291	2	(Scott et al., 2015)
US-SRM	31.8	-110.9	2004	2014	WSA	BSk	1120	5	(Scott et al., 2009)
US-Syv	46.2	-89.4	2001	2014	MF	Dfb	540	6	(Desai et al., 2005)
US-Ton	38.4	-121.0	2001	2014	WSA	Csa	177	8	(Ma et al., 2016)
US-Twt	38.1	-121.7	2009	2014	CRO	Csa	-7	5	(Pastorello et al., 2020)
US-UMB	45.6	-84.7	2000	2014	DBF	Dfb	234	10	(Gough et al., 2008)
US-Var	38.4	-121.0	2000	2014	GRA	Csa	129	9	(Ma et al., 2011)

US-WCr	45.8	-90.1	2000	2014	DBF	Dfb	520	4	(Cook et al., 2004)
US-Whs	31.7	-110.1	2011	2013	OSH	BSk	1370	10	(Pastorello et al., 2020)
US-Wi4	46.7	-91.2	2007	2014	ENF	Dfb	352	7	(Noormets et al., 2007)
US-Wi9	46.6	-91.1	2002	2005	ENF	Dfb	350	1	(Noormets et al., 2007)
US-Wkg	31.7	-109.9	2004	2005	GRA	BSk	1531	8	(Scott, 2010)
US-WPT	41.5	-83.0	2004	2014	WET	Cfa	175	3	(Pastorello et al., 2020)
US-Wrc	45.8	-122.0	2000	2006	ENF	Csb	371	1	(Wharton et al., 2012)
ZA-Kru	-25.0	31.5	2000	2012	SAV	BSh	359	3	(Archibald et al., 2009)
ZM-Mon	-15.4	23.3	2007	2009	WSA	Aw	1053	9	(L. Merbold et al., 2009)

Note.

[*a]: collected from (Flechard et al., 2020).

[*b]: collected from (Hao et al., 2019).

[*c]: collected from (B. Tang et al., 2018).

[*d]: collected from (X. Tang et al., 2020).

[*e]: extracted from google earth.

Other elevation data were collected from https://fluxnet.org/, http://www.europe-fluxdata.eu/, http://www.ozflux.org.au/, https://ameriflux.lbl.gov/, http://www.asiaflux.net/, http://www.chinaflux.org/, and ancillary information of LaThuile dataset (https://fluxnet.org/data/la-thuile-dataset/).

Table S2. List of the forcing variables for the LUE model. The variables in bold are used to calibrate the model parameters.

Abbreviation	Definition	Unit	Equation or source	Reference
LE	Latent heat flux, 'LE_F_MDS' in FLUXNET2015 dataset or 'LE_f' in LaThuile dataset	$MJ \cdot m^{-2} \cdot d^{-1}$	EC observations	See Table S1
NEE	Net ecosystem exchange, 'NEE_VUT_REF' or 'NEE_f'	$gC \cdot m^{-2} \cdot d^{-1}$	EC observations	
Precip	Precipitation, 'P_F' or 'precip'	mm	EC observations	

QA	Quality flag of the variable from EC measurement, e.g., 'SW_IN_F_QC' is the QA of global radiation in FLUXNET2015 dataset, and 'Rg_fqcOK' is QA of that in LaThuile dataset.	Unitless (0-1)	FLUXNET dataset	(Pastorello et al., 2020)
QC	Quality flags for all the reflectance of MCD43A4 product	Unitless	MCD43A2 quality assessment product	(Schaaf & Wang, 2015)
R_g^a	Global radiation, 'SW_IN_F' or 'Rg_f'	$MJ \cdot m^{-2} \cdot d^{-1}$	EC observations	
R_p^a	Potential radiation, 'SW_IN_POT' or 'Rg_pot'	$MJ \cdot m^{-2} \cdot d^{-1}$	EC observations	See Table S1
R_n^a	Net radiation, 'NETRAD' or 'Rn_f'	$MJ \cdot m^{-2} \cdot d^{-1}$	EC observations	
r_{red}	Reflectance at red band	Unitless (0-1)	MCD43A4 version 6 Nadir BRDF-Adjusted Reflectance product	(Schaaf & Wang, 2015)
r_{nir}	Reflectance at near-infrared band	Unitless (0-1)	As above	
T^a	Air temperature, 'TA_F' or 'Tair_f'	°C	EC observations	See Table S1
VPD^a	Vapor pressure deficit, 'VPD_F' or 'VPD_f'	kPa	EC observations	See Table S1
CI	Cloudiness index	Unitless (0-1)	$1-R_g/R_p$	(Fu & Rich, 1999; Turner et al., 2006)
CO_2	Atmospheric CO_2 concentration	ppm	Observations by NOAA/ESRL. The global annual mean atmospheric CO_2 concentration was converted to daily time steps using a linear interpolation function	www.esrl.noaa.gov/ gmd/ccgg/trends/
$\mathbf{ET_{obs}}^d$	Evapotranspiration	mm	converted from LE using a latent heat of vaporization changing with T	(Henderson - Sellers, 1984)
PET	Potential ET	mm	Estimated using Rn and T	(Priestley & Taylor, 1972)

GPP_{obs}[d]	Gross primary productivity, 'GPP_NT_VUT_REF' or 'GPP_f'	$gC \cdot m^{-2} \cdot d^{-1}$	Estimated from NEE using the night-time partitioning method	(Reichstein et al., 2005)
NDVI[c]	MODIS-based Normalized differential vegetation index	Unitless (-1-1)	$\frac{r_{nir}-r_{red}}{r_{nir}+r_{red}}$	(Rouse et al., 1974)
PAR	Photosynthetically active radiation	$MJ \cdot m^{-2} \cdot d^{-1}$	$R_g \times 0.45$	(Running & Zhao, 2015; Weiss & Norman, 1985)
WAI	Water availability index	mm	Estimated using Precip and PET, with two site-level calibrated parameters	See the algorithm of WAI in (Boese et al., 2019; Tramontana et al., 2016) and detailed calibration process in section S1 in (Bao et al., 2022)
W	Soil water supply	Unitless (0-1)	$W = \min(1, WAI/AWC)$	(Bao et al., 2022)
σ_{LE}	Random uncertainty of ET, 'LE_RANDUNC' or 'LE_fsd_UncNew_fullDay_m1'	$MJ \cdot m^{-2} \cdot d^{-1}$	Standard deviation of LE	(Pastorello et al., 2020)
σ_{NEE}	Random uncertainty of GPP, 'NEE_VUT_REF_RANDUNC' or 'NEE_fsd_UncNew_fullDay_m1'	$gC \cdot m^{-2} \cdot d^{-1}$	Standard deviation of NEE	
FAPAR[b]	Fraction of absorbed PAR	Unitless (0-1)	$\begin{cases} = NDVI\ (NDVI>0) \\ = 0\ (NDVI \leq 0) \end{cases}$	(Myneni et al., 1997)

Note. All the above variables are at the daily scale;

[a]The gaps in the R_g, R_p, R_n, T, and VPD were filled using machine-learning-based downscaling (Besnard et al., 2019) of gridded product from CRUNCEP (Viovy, 2018);

[b]The linear relationship between FAPAR and NDVI was assumed according to (Myneni et al., 1997).

[c]The gaps in NDVI was filled using FluxnetEO dataset (Walther et al., 2022). The time-series NDVI were filtered by Savitzky-Golay filter (window size was eleven and polynomial order was three) (Savitzky & Golay, 1964).

[d]Since GPP_{obs} is estimated from NEE and ET_{obs} is estimated from LE, the QA of GPPobs and ETobs are represented by QA of NEE ('NEE_VUT_REF_QC' or 'NEE_fsd_UncNew_fullDay_m1') and LE ('LE_F_MDS_QC' or 'LE_fsd_UncNew_fullDay_m1'), respectively.

Table S3. Eddy covariance flux site list used in this study. The latitude (Lat), longitude (Lon) and plant functional types (PFT) are collected from FLUXNET website. The data length differs

across site and is determined by the years between 'data start' and 'data end'. The climate type is extracted from the Koeppen-Geiger climate classification map (at 5 arc min; Rubel et al., 2017). The elevation is collected from the site ancillary information, papers and satellite images (see the footnote below the table). The site group refers to the group number of each site used to validate the training result.

Class name	Short names	Definitions	References
PFT	PFT	Plant functional types	See Table S1, eleven types in total
Clim	Clim	Koeppen-Geiger climate classification types	See Table S1, five main climate types and fourteen specific classification types in total
BioClim	BIO1	Annual Mean Temperature	Calculated based on the ANUCLIM algorithm (Xu & Hutchinson, 2011) using CRUNCEP dataset (Viovy, 2018) from 1986-2015.
	BIO2	Mean Diurnal Range (Mean of monthly maximum temperature minus minimum temperature)	
	BIO3	Isothermality (BIO2 divided by BIO7 and 100)	
	BIO4	Temperature Seasonality (standard deviation of temperature multiply with 100)	
	BIO5	Max Temperature of Warmest Month	
	BIO6	Min Temperature of Coldest Month	
	BIO7	Temperature Annual Range (BIO5 minus BIO6)	
	BIO8	Mean Temperature of Wettest Quarter	
	BIO9	Mean Temperature of Driest Quarter	
	BIO10	Mean Temperature of Warmest Quarter	
	BIO11	Mean Temperature of Coldest Quarter	
	BIO12	Annual Precipitation	
	BIO13	Precipitation of Wettest Month	
	BIO14	Precipitation of Driest Month	
	BIO15	Precipitation Seasonality (Coefficient of Variation)	
	BIO16	Precipitation of Wettest Quarter	
	BIO17	Precipitation of Driest Quarter	
	BIO18	Precipitation of Warmest Quarter	
	BIO19	Precipitation of Coldest Quarter	
	AI1	Mean annual aridity index (ratio between mean annual precipitation and potential evapotranspiration)	Calculated using the CRUNCEP dataset from 1986-2015
	AI2	Seasonality of aridity index (standard deviation of mean monthly aridity index)	

VIF	VIF1	Annual mean EVI (enhanced vegetation index)	Calculated based on the bioclimatic variables (BIO1-BIO11) algorithm using the gap-filled Landsat-based EVI (Walther et al., 2022) from 1986-2015
	VIF2	Mean monthly EVI range	
	VIF3	Mean EVI variability (VIF2 divided by VIF7)	
	VIF4	EVI seasonality (standard deviation of EVI)	
	VIF5	Max EVI of Warmest Month	
	VIF6	Min EVI of Coldest Month	
	VIF7	Annual EVI Range (BIO5 minus BIO6)	
	VIF8	Mean EVI of Wettest Quarter	
	VIF9	Mean EVI of Driest Quarter	
	VIF10	Mean EVI of Warmest Quarter	
	VIF11	Mean EVI of Coldest Quarter	
NPdep	$Ndep_{NHX}$	Average atmospheric nitrogen deposition (NH_3 and NH_4)	Extracted from the product of the atmospheric chemistry transport model TM3 (Wang et al., 2017)
	$Ndep_{NOY}$	Average atmospheric nitrogen deposition (NO and NO_2)	
	Pdep	Average atmospheric phosphorus deposition	
Soil	BDRICM	Depth to bedrock (R horizon) up to 200 cm	Extracted from the Soil Grids product (Poggio et al., 2021)
	BDRLOG	Probability of occurrence (0-100%) of R horizon	
	BDTICM	Absolute depth to bedrock (in cm)	
	BLDFIE	Bulk density (fine earth) in kg/m3 at depth 0.00 m	
	CECSOL	Cation exchange capacity of soil in cmol/kg at depth 0.00 m	
	CLYPPT	Clay content (0-2 micro meter) mass fraction in % at depth 0.00 m	
	CRFVOL	Coarse fragments volumetric in % at depth 0.00 m	
	ORCDRC	Soil organic carbon content (fine earth fraction) in g/kg at depth 0.00 m	
	PHIHOX	Soil pH*10 in H2O at depth 0.00 m	
	PHIKCL	Soil PH*10 in KCl at depth 0.00 m	
	SLTPPT	Silt content (2-50 micro meter) mass fraction in % at depth 0.00 m	
	SNDPPT	Sand content (50-2000 micro meter) mass fraction in % at depth 0.00 m	
	AWCh1	Derived available soil water capacity (volumetric fraction) with FC = pF 2.0 for	

	depth 0 cm
AWCh2	Derived available soil water capacity (volumetric fraction) with FC = pF 2.3 for depth 0 cm
AWCh3	Derived available soil water capacity (volumetric fraction) with FC = pF 2.5 for depth 0 cm
WWP	Derived available soil water capacity (volumetric fraction) until wilting point for depth 0 cm
AWCtS	Saturated water content (volumetric fraction) teta-S for depth 0 cm